



Horizontal distribution of tropospheric NO₂ and aerosols derived by dual-scan multi-wavelength MAX-DOAS measurements in Uccle, Belgium

Ermioni Dimitropoulou¹, François Hendrick¹, Martina M. Friedrich¹, Frederik Tack¹, Gaia Pinardi¹,
5 Alexis Merlaud¹, Caroline Fayt¹, Christian Hermans¹, Frans Fierens² and Michel Van Roozendael¹

¹Royal Belgian Institute for Space Aeronomy (BIRA-IASB), Brussels, 1180, Belgium

²IRCEL-CELINE, Brussels, Belgium

Correspondence to: Ermioni Dimitropoulou (ermioni.dimitropoulou@aeronomie.be)

Abstract

10 Dual-scan ground-based Multi-AXis Differential Optical Absorption Spectroscopy (MAX-DOAS) measurements of tropospheric nitrogen dioxide (NO₂) and aerosols were carried out in Uccle (50.8°N, 4.35°E; Brussels region, Belgium) for two years, from March 2018 to February 2020. The MAX-DOAS instrument was operating in both UV and Visible wavelength ranges in a dual-scan configuration consisting of two sub-modes: (1) an elevation scan in a fixed viewing azimuthal direction and (2) an azimuthal scan in a fixed low elevation angle (2°). By analyzing the O₄ and NO₂ dSCDs at six different wavelength
15 intervals along every azimuthal direction and by applying a new Optimal-Estimation-based inversion approach, the horizontal distribution of the NO₂ near-surface concentrations and vertical column densities (VCDs) and the aerosols near-surface extinction coefficient are retrieved along ten azimuthal directions. The retrieved horizontal NO₂ concentration profiles allow the identification of the main NO₂ hotspots in the Brussels area. Correlative comparisons of the retrieved horizontal NO₂ distribution were conducted with airborne, mobile, and satellite datasets, and overall a good agreement is found. The
20 comparison with TROPOMI observations reveals that the characterization of the horizontal distribution of tropospheric NO₂ VCDs by ground-based measurements, the appropriate sampling of TROPOMI pixels, and an adequate a priori NO₂ profile shape in TROPOMI retrievals lead to a better consistency between satellite and ground-based datasets.

1 Introduction

Aerosols and nitrogen dioxide (NO₂) play a crucial role in the tropospheric chemistry. NO₂ is an important tropospheric
25 pollutant mainly emitted by combustion processes and nitrogen fertilizers used in agriculture (Seinfeld and Pandis, 1998). Traffic, domestic heating, industrial activities, and power plants are the largest NO₂ emitters (Tack et al., 2021). Beyond its harmful effects on human health (Chen et al., 2007), NO₂ participates in the formation of tropospheric ozone (O₃) by a non-linear photochemical mechanism which involves volatile organic compounds (VOCs).



30 Aerosols with small diameter are estimated to cause millions of premature deaths per year globally because of their ability to penetrate deeply into the lungs (Khomenko et al., 2021). Aerosols influence the Earth's climate system by changing its radiation budget by scattering and absorbing sunlight (Quaas et al., 2008). In the boundary layer of urban regions, the horizontal distribution of NO₂ is highly heterogeneous given the fact that it is a short-lived species (Beirle et al., 2003). For those reasons, the regional and global monitoring of NO₂ and aerosols at high spatial resolution is crucial.

35 Since 1995, with the ERS-2 GOME (Global Ozone Monitoring Experiment) instrument (Burrows et al., 1999), satellite nadir air-quality measurements of atmospheric backscattered sunlight in the UV-visible range have provided daily global tropospheric column measurements of numerous trace gases, such as NO₂. Many satellite missions dedicated to air-quality monitoring followed over the next years with increasing spatial resolution. More recently, the Tropospheric Monitoring Instrument (TROPOMI) sensor launched onboard the Sentinel-5P Precursor (S5P) platform in October 2017 reached an initial spatial resolution of 7x3.5 km², and augmented on 6 August 2019 to 5.5x3.5 km². Due to TROPOMI's fine spatial resolution, 40 monitoring the horizontal distribution of NO₂ in urban regions and identifying specific emission sources is made easier than with previous satellite missions but still, TROPOMI cannot fully capture the fine-scale (sub-kilometer) structures in the effective NO₂ field. Consequently, TROPOMI requires further attention concerning its measurements validation.

Tropospheric vertical columns of many trace gases like NO₂, formaldehyde (HCHO), sulphur dioxide (SO₂), nitrous acid (HONO) and O₃ can be retrieved by the Multi-AXis Differential Optical Absorption Spectroscopy (MAX-DOAS) technique 45 (Hönninger et al., 2004; Wittrock et al., 2004; Pinaridi et al., 2008, 2013; Clémer et al., 2010; Hendrick et al., 2014; Irie et al., 2011, 2012; Sinreich et al., 2007; Wagner et al., 2011; Wang et al., 2018). In recent years, MAX-DOAS measurements have been widely used as reference datasets for the validation of nadir airborne and space-borne air-quality measurements. MAX-DOAS instruments measure the scattered sunlight in the UV and Visible spectral ranges at multiple elevation angles above the horizon. For absorbers located close to the surface, such as tropospheric NO₂, the higher sensitivity is achieved for low MAX- 50 DOAS elevation angles. During the last years, MAX-DOAS measurements in more than one azimuthal direction are emerging (Ortega et al., 2016; Wang et al., 2014; Chan et al., 2020; Schreier et al., 2021). Multi-azimuthal MAX-DOAS measurements offer many possibilities on air-quality monitoring, such as a better characterization of the effective NO₂ field around the station. These ground-based datasets can be valuable for validating satellite missions with fine spatial resolution in regions where the NO₂ horizontal distribution is heterogeneous, such as urban and sub-urban areas.

55 In this study, a new aerosol and NO₂ horizontal distribution inversion approach based on two years (March 2018-February 2020) of dual-scan multi-wavelength MAX-DOAS measurements in Uccle (Brussels-Capital region, Belgium) is presented. In every azimuthal viewing direction, parameterized NO₂ near-surface concentrations, NO₂ tropospheric columns and aerosol extinctions measured at six different wavelengths are used as input in a new horizontal distribution inversion approach. On this basis, the near-surface aerosol extinction and NO₂ horizontal distributions are retrieved at a spatial resolution of about 60 3km in a range of about 20 km around the measurement site. These horizontal profiles are used to validate collocated TROPOMI tropospheric NO₂ columns. One complete year of data (March 2018-March 2019) and two wavelength intervals (one in the UV and one in the Visible) have already been used in Dimitropoulou et al. (2020). It is proven that multi-azimuthal



(the so-called dual-scan) MAX-DOAS measurements significantly improve the agreement between ground-based and TROPOMI tropospheric NO₂ column observations over the Brussels' area. By adding the multi-wavelength aspect, the present work represents an extension of the former study.

The manuscript is organized into six sections: in Sect. 2, the measurement site with the MAX-DOAS experimental set-up and the multi-wavelength DOAS analysis are presented. In Sect. 3, the TROPOMI tropospheric NO₂ measurements are described. Section 4 is composed of two main parts: Sect. 4.1 is a detailed description of the dual-scan multi-wavelength MAX-DOAS retrieval method and Sect. 4.2 is the horizontal aerosol and NO₂ distribution inversion approach. In Sect. 5, main results followed by correlative comparisons of the retrieved ground-based and satellite horizontal NO₂ distribution are presented. Finally, in Sect. 6, conclusions and future perspectives are given.

2 Dual-scan multi-wavelength MAX-DOAS measurements

2.1 Measurement site and experiment set-up

Brussels-Capital Region is the most densely populated area in Belgium, where pollutant concentrations, such as NO₂, are often high because of anthropogenic activities (Tack et al., 2021).

A MAX-DOAS dual-scan instrument was operated by BIRA-IASB (Koninklijk Belgisch Instituut voor Ruimte-Aeronomie – Institut Royal d'Aeronomie Spatiale de Belgique) in Uccle from January 2017 to February 2020. Uccle is located to the South of the city-center of Brussels and to the West of a large forested area (Bois de la Cambre). Therefore, it is an ideal site to perform MAX-DOAS observations under moderate to high pollution level conditions. Additionally, the characterization of the horizontal distribution of NO₂ and aerosols at high spatial resolution is of great interest here because of the heterogeneity of the pollution sources (car traffic, national airport, power plant) in the capital region of Brussels.

The MAX-DOAS dual-scan instrument is composed of the following parts: the optical head mounted on a sun tracker, two spectrometers (UV and Visible) inside a thermo-regulated box and the data-acquisition unit. The optical head and the two spectrometers are connected with optical fibers. A more detailed description of the BIRA-IASB MAX-DOAS dual-scan instrument can be found in Dimitropoulou et al. (2020).

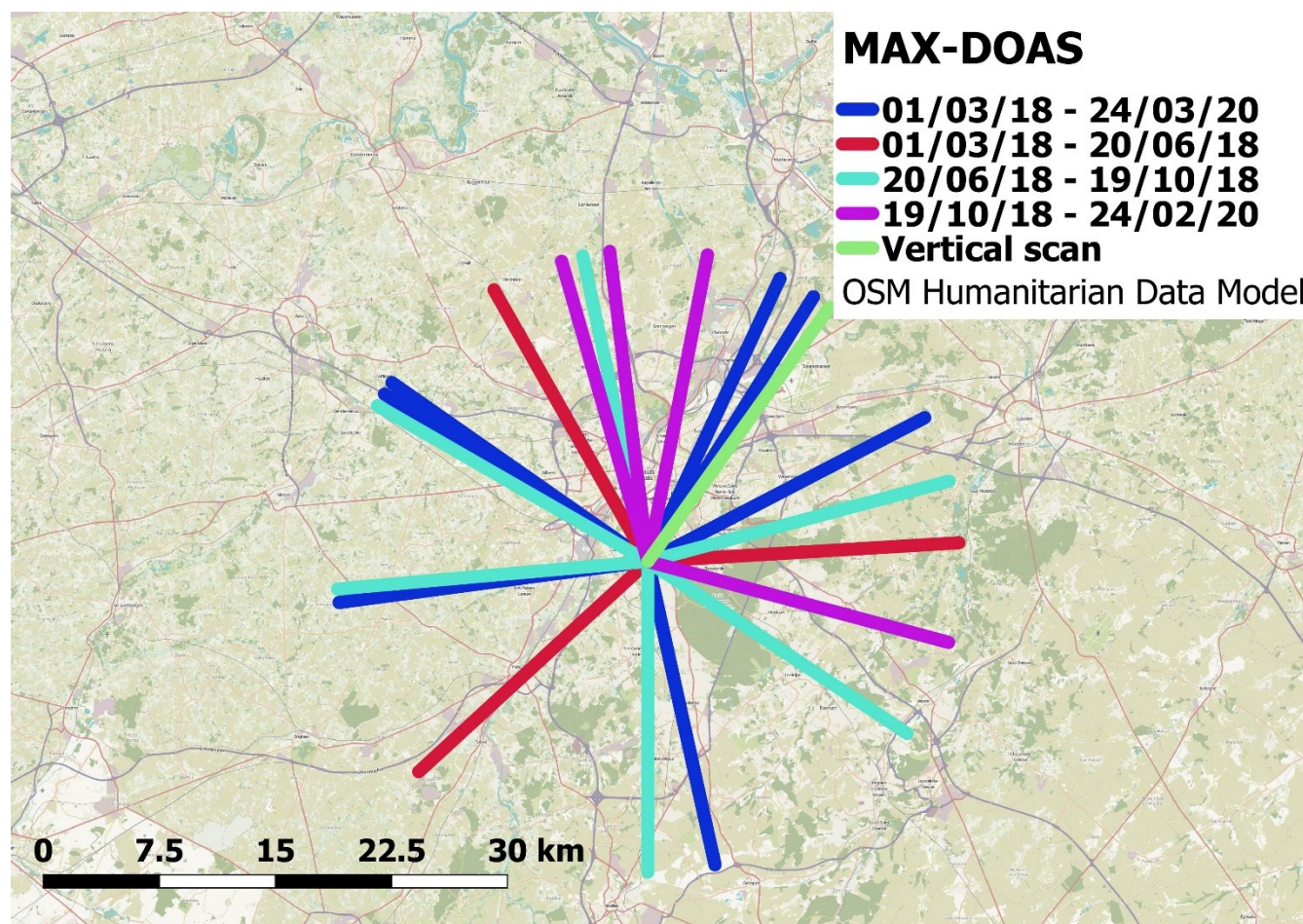
From March 2018 to February 2020, the MAX-DOAS instrument operated in a dual-scan viewing mode. Two different sub-modes compose one complete measurement scan (see Dimitropoulou et al., 2020): (1) a vertical scan in nine different elevation angles (EAs) in one fixed telescope azimuthal direction (TAA; Northeast direction i.e., towards the city center and the national airport) and (2) a horizontal scan in nine different azimuthal directions at a fixed elevation angle (2° above the horizon).

Several azimuthal viewing directions were tested to obtain an optimal horizontal sampling without any obstacle in the different viewing directions (see Fig. 1). The selection of more azimuthal directions towards the North, Northeast, and Northwest directions was made considering the location of the main NO₂ emission sources and, consequently, the highly variable NO₂ horizontal distribution towards these directions.

The integration time for each measured radiance spectrum is 60s, resulting in a full scan duration of approximately 20 minutes.



95



100 **Figure 1.** The experimental set-up of the BIRA-IASB dual-scan MAX-DOAS instrument. Each line is color-coded according to the different set-ups that were used from March 2018 to February 2020. The length of each line is equal to 20 km, which corresponds to the typical horizontal sensitivity for the MAX-DOAS measurements in the present study (see Fig. 18). © OpenStreetMap contributors 2021. Distributed under the Open Data Commons Open Database License (ODbL) v1.0.

2.2 Multi-wavelength DOAS analysis

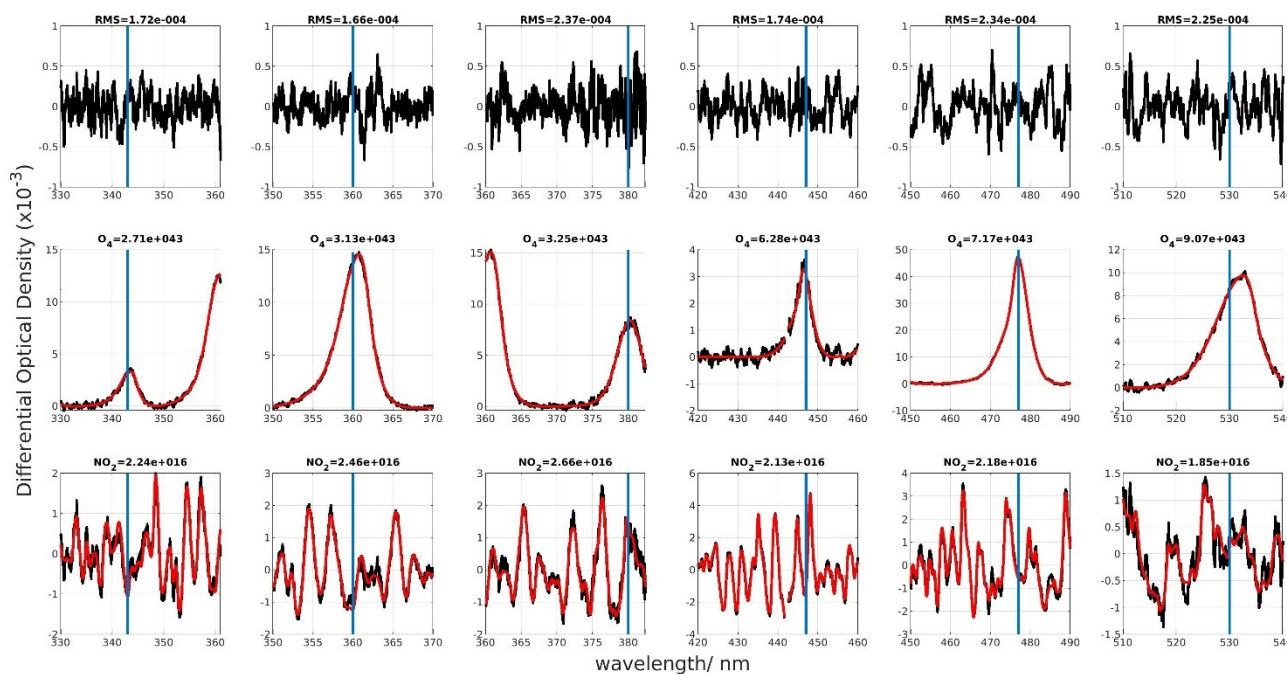
105 The measured radiance spectra of a full measurement scan are analyzed using the QDOAS spectral fitting software developed by BIRA-IASB (Fayt et al., 2011). The DOAS technique separates the narrow absorption features of trace gases in the UV-Visible spectral range from a spectral background caused mainly by Mie and Rayleigh scattering and instrumental effects. The



110 trace gas concentration integrated along the light-path in a measured spectrum relative to the amount of the same absorber in
a reference spectrum is the primary product of the DOAS analysis and is called differential slant column density (dSCD). Here,
average zenith spectra before and after each measurement scan are used as a reference.

The O₄ and NO₂ dSCDs are retrieved in six different wavelength intervals: Three intervals in the UV spectral range (330-361
nm, 350-370 nm, and 360-383.5 nm) and three in the Visible range (420-460 nm, 450-490 nm, and 510-540.1 nm). These
fitting windows were selected to optimize the determination of the O₄ and NO₂ dSCDs at the maximum number of different
O₄ absorption bands available in the wavelength domain of the instrument. Figure 2 shows an example of the O₄ and NO₂ fits
115 in all the intervals used in the present work. In each chosen fitting window, we select a reference wavelength, which
corresponds to the maximum of an O₄ absorption peak (or close to it) in the respective wavelength intervals (see Fig. 2), and
it is subsequently used for radiative transport calculations and further analysis. The different reference wavelengths are 343
nm, 360 nm, 380 nm, 447 nm, 477 nm and 530 nm (see Fig. 2). To optimize the derivation of the dSCDs at the six selected
wavelengths, the fit of a slope parameter, which accounts for the variation of the dSCD within the fitting interval (Puķīte et
120 al., 2010), is necessary. This is especially important when the reference wavelength is not located in the center of the fitting
window (i.e., 330-361 nm, 350-370 nm, 420-460 nm, and 450-490 nm). The DOAS settings used for each fitting interval are
presented in Table S1. As shown in this table, two different O₄ cross-sections are used in this study: (1) Finkenzeller (private
communication) in the UV fitting intervals and (2) Thalman and Volkamer, (2013) in the Vis fitting intervals. The main
motivation for using the O₄ cross-section from Finkenzeller (measured at 25°C) in the UV fitting intervals is the significant
125 improvement of the fit quality and the reduction of the uncertainties for the UV retrievals. Sensitivity tests and comparisons
with radiative transport simulations also show that the resulting O₄ and NO₂ dSCDs are consistent throughout the whole
wavelength range covered by the six intervals. For NO₂ and O₃, which are the strongest absorbers in all the fitting windows,
a correction for the solar I₀ effect (Aliwell et al., 2002) is applied. A high-resolution solar atlas (Kurucz et al., 1984) is used
for the wavelength calibration of the measured spectra.

130



135 **Figure 2.** Fit results of the O_4 and NO_2 fit at the six selected fitting windows from the dual-scan MAX-DOAS measurements in Uccle (2 June 2019 at 07:05 UTC). The measured spectra are represented with black lines, while the fit results are shown with red lines. The blue lines represent the six reference wavelengths.

3 TROPOMI tropospheric NO_2 measurements

In the present study, MAX-DOAS tropospheric NO_2 VCDs are used to validate collocated TROPOMI satellite observations. TROPOMI is a passive grating imaging spectrometer flying onboard the S5P satellite platform. It covers the UV-Visible (250-500 nm), near-infrared (710-770 nm), and short-wave infrared (2314-2382 nm) spectral ranges (Veefkind et al., 2011). TROPOMI measures in a push-broom configuration with a full swath width as wide as 2600 km, and it provides daily global coverage at a spatial resolution (true-nadir pixel size) of 7×3.5 km², further improved to 5.5×3.5 km² on 6 August 2019. The TROPOMI tropospheric NO_2 algorithm has been developed at KNMI and uses a retrieval-assimilation-modeling system that is based on the 3-D global TM5 chemistry transport model (van Geffen et al., 2019; Williams et al., 2017).

We use the reprocessed (RPRO) and offline (OFFL) datasets of the TROPOMI L2 tropospheric NO_2 column product (see Table 1 for the corresponding versions). According to the guidelines provided by van Geffen et al. (2019), RPRO dataset are available only for the first period of the present study (see Table 1). For the remaining periods, OFFL datasets are used, which are the main data products being available within two weeks from the TROPOMI measurement. To ensure best measurements' quality, only pixels with a quality assurance value larger than 0.75 are used. This quality flagging eliminates pixels with a cloud radiance fraction larger than 0.5, snow or ice, and erroneous retrievals.



Next to operational products, two additional TROPOMI data sets are also used (see Section 5). In the first one, the TROPOMI retrieval is performed with different a priori profiles (Douros et al., in preparation). The coarse TM5-MP a priori NO₂ profiles, using a spatial resolution of 1° x 1°, is replaced by NO₂ profile shapes from the CAMS (Copernicus Atmospheric Monitoring Service) regional Chemistry Transport Model (CTM) ensemble at a spatial resolution of 0.1° x 0.1°. The replacement of a coarse a priori information by a finer one can lead to significant changes in the TROPOMI retrieved NO₂ tropospheric columns. The available dataset covers October 2018 to March 2020 (OFFL dataset, L2, and version 01.03.01, 01.03.02, and 02.00.00). In the second additional product, the TROPOMI retrieval is performed with an improved cloud product (Eskes et al., 2021; van Geffen et al., 2021). According to van Geffen et al. (2021), the improvement in the FRESCO-S cloud pressure retrieval scheme to the FRESCO-wide product, has an impact on the NO₂ AMFs and consequently, on the NO₂ tropospheric columns over polluted areas. More precisely, the existing FRESCO-S product had a negative bias in the cloud top pressure values, which resulted in a low NO₂ tropospheric column (Compernelle et al., 2020). The TROPOMI tropospheric NO₂ columns are retrieved using an improved FRESCO-S cloud retrieval scheme, called FRESCO-wide, in v1.4 since 29 November 2020. In the present study, the diagnostic data sets (DDS) are used, which are an ensemble of reprocessed data for past periods analyzed with new versions (van Geffen et al., in preparation). Over the MAX-DOAS measurement time-period, only DDS2 data corresponding to OFFL datasets (v1.2 and v1.3) are available. Excluding the spin-up period needed by TM5-MP, only four data periods are available for our comparisons (i.e., 30/06/2018 - 06/07/2018, 30/12/2018 - 5/01/2019, 30/03/2019-05/04/2019, and 17/09/2019-23/09/2019).

170 **Table 1. TROPOMI NO₂ processor versions used in the present study.**

| Dataset | Version | Starting date | End date |
|---------|----------|---------------|------------|
| RPRO | 01.02.02 | 30/04/2018 | 17/10/2018 |
| OFFL | 01.02.00 | 17/10/2018 | 28/11/2018 |
| OFFL | 01.02.02 | 28/11/2018 | 20/03/2019 |
| OFFL | 01.03.00 | 20/03/2019 | 30/04/2019 |
| OFFL | 01.03.01 | 23/04/2019 | 26/06/2019 |
| OFFL | 01.03.02 | 26/06/2019 | 24/02/2020 |

4 Description of the dual-scan multi-wavelength MAX-DOAS inversion approach

First, the measured radiance spectra in the UV and Visible wavelength ranges is analyzed in six different fitting windows with the main output being the O₄ and NO₂ dSCDs at six wavelengths, which are 343 nm, 360 nm, 380 nm, 447 nm, 477 nm and 530 nm (see Section 2.2). Then, the OEM-based MMF algorithm is applied to the O₄ and NO₂ dSCDs in the main azimuthal



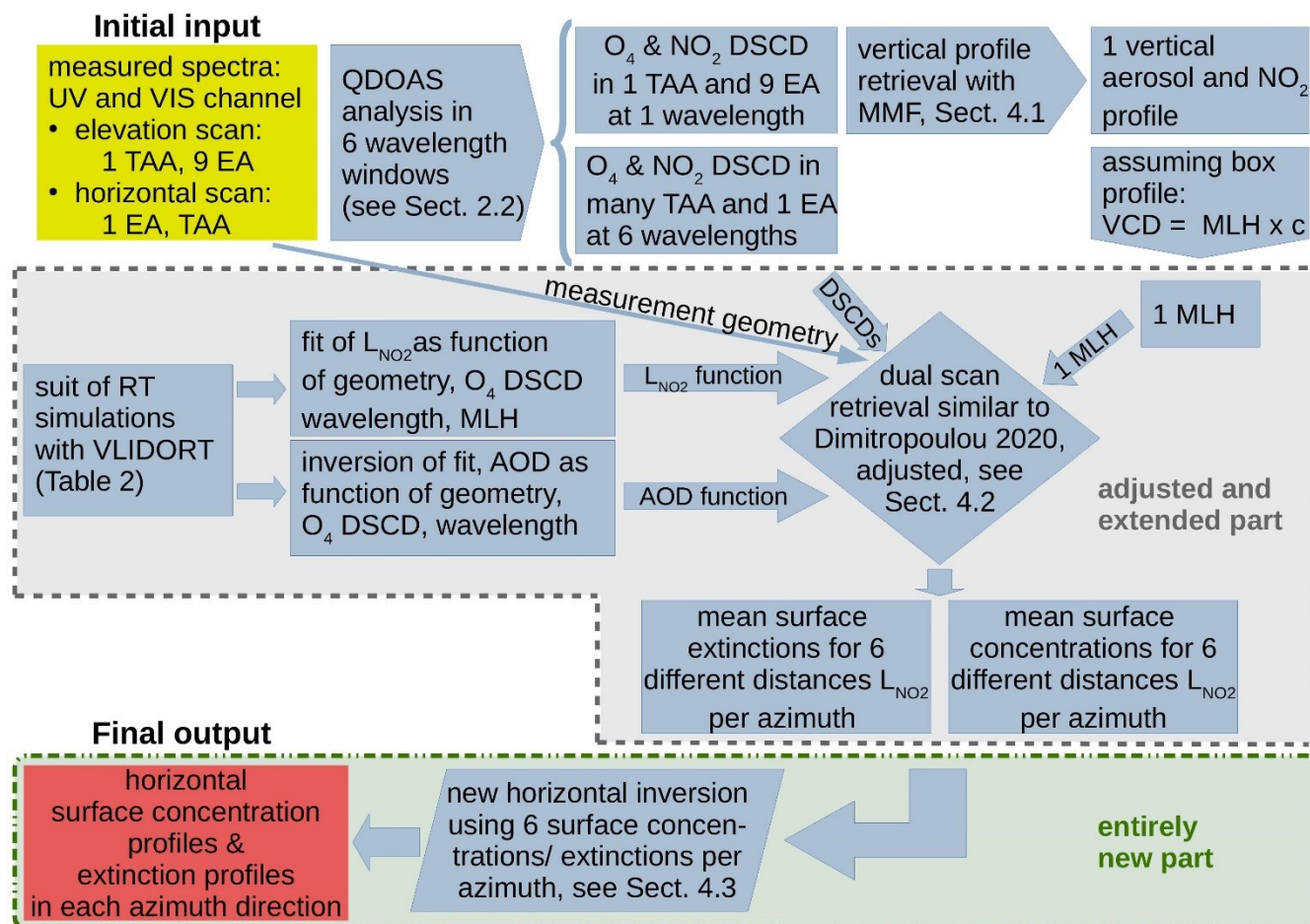
direction (and at 477 nm) to retrieve vertical NO_2 profiles and obtain information about the vertical extent of NO_2 in the troposphere (MLH_{NO_2} ; see Section 4.1).

As an intermediate step, radiative transfer model (RTM) simulations are performed (see Table 2 and Section 4.2) to obtain information about the horizontal sensitivity (L_{NO_2}) and AOD as a function of O_4 dSCDs, wavelength, and MLH_{NO_2} .

180 Then, in the next step, a new dual-scan parameterization technique is applied to the O_4 and NO_2 dSCDs at the six different wavelengths and in all the azimuthal directions with MLH_{NO_2} , measured O_4 dSCDs, and measurement geometry being the main input parameters to retrieve the horizontal sensitivity of NO_2 and, consequently, the NO_2 near-surface concentrations and VCDs, and near-surface aerosol extinction (see Section 4.2).

In the final step, a new OEM-based horizontal distribution inversion approach is developed using the six near-surface NO_2
 185 concentrations and aerosol extinction values per azimuthal direction to retrieve horizontal NO_2 and aerosol extinction horizontal profiles in an output horizontal grid of 500m thickness (see Section 4.3).

A flow chart describing the dual-scan multi-wavelength MAX-DOAS inversion approach is shown in Fig. 3.





190 **Figure 3. Dual-scan multi-wavelength MAX-DOAS inversion approach flow chart.**

4.1 Aerosol and NO₂ OEM-based profile retrievals

The Optimal-estimation-based Mexican MAX-DOAS Fit (MMF) inversion algorithm (Friedrich et al., 2019) is applied to retrieve the aerosol extinction coefficient and NO₂ vertical profiles for each MAX-DOAS elevation scan in the main azimuthal direction at 360 nm and 477 nm. First, the O₄ measurements are used to retrieve the aerosol extinction profile. Several studies indicated the importance of applying a scaling factor (<1) to the observed O₄ dSCDs to bring them in agreement with simulated O₄ dSCDs by radiative transfer modeling (see Wagner et al., 2019 / Table 1 for a comprehensive list of all those studies). However, there is no consensus on the fundamental reason for applying this scaling (see e.g. Ortega et al., 2016). As found by Tirpitz et al. (2021), the choice of the scaling factor has only a small effect on the performance of the trace gas retrieval, so we decided not to apply it in the present study. The aerosol extinction profile retrieved from each scan is used as an input to the radiative transfer calculations used to retrieve the NO₂ retrieval profile. Further details about the MMF inversion algorithm, the input a priori parameters, the quality check of each scan, and the estimated uncertainties of the aerosol and NO₂ vertical profile can be found in Dimitropoulou et al. (2020).

205 A broken cloud-filtering approach based on Gielen et al. (2014) is applied to the MAX-DOAS measurements to exclude MAX-DOAS aerosol and NO₂ scans influenced by the presence of clouds, which are known to potentially degrade the quality of the retrievals (Gielen et al. 2014, Wagner et al. 2014). Three sky conditions can be distinguished with this flagging approach: (1) clear sky, (2) homogeneous cloud coverage and (3) broken clouds conditions. Retrievals under broken cloud conditions are rejected from the present study.

210 The profile retrieval was performed to estimate the Mixing Layer Height of NO₂ (MLH_{NO₂}). The MLH_{NO₂} is estimated per measurement scan, and it is the ratio of VCD_{NO₂} to the NO₂ near-surface concentration as retrieved in the main azimuthal direction by the MMF inversion algorithm. Therefore, during one measurement scan, two assumptions were made: (1) the homogeneous distribution of NO₂ inside the MLH_{NO₂} and (2) the homogeneous MLH_{NO₂} around the measurement site and its use in all the azimuthal directions. The validity of the second assumption is tested in Sect. 4.2.2.

215

4.2 Dual-scan MAX-DOAS retrieval method

A complete MAX-DOAS measurement scan is composed of two different sub-scans, as described in Sect. 2.1. The aerosol and NO₂ vertical profiles are retrieved from the elevation scan in the main azimuthal direction. In the other azimuthal directions, measurements are performed only in a single low elevation angle (2°), and therefore, the retrieval of aerosol and NO₂ vertical profiles is not possible. Using the fact that the lowest elevation angles have the highest sensitivity to trace gases located nearby the surface due to the long light path in this layer, a new dual-scan MAX-DOAS retrieval strategy was



developed here. This new retrieval strategy is an extension of the work presented in Dimitropoulou et al. (2020) and aims to retrieve the near-surface NO₂ box-averaged volume mixing ratios (VMRs) and the NO₂ VCDs at six different wavelengths. In Dimitropoulou et al. (2020), the applied dual-scan NO₂ MAX-DOAS retrieval was itself an adaptation of the parameterization technique proposed by Sinreich et al. (2013). More precisely, in the presence of sufficient aerosols in the atmosphere (i.e., sufficient aerosols to constrain the light path in a near-surface layer and ensure that the near-surface NO₂ concentration can be approximated by a near-surface box profile), the measured NO₂ dSCDs at one low elevation angle (2°) can be related to the near-surface NO₂ box-averaged concentration as follows:

$$230 \quad \text{dSCD}_{\text{NO}_2} = c_{\text{NO}_2} L_{\text{NO}_2} \quad (1)$$

where $\text{dSCD}_{\text{NO}_2}$ is the differential slant column density of NO₂ and c_{NO_2} its mean concentration along the differential effective light path, L_{NO_2} .

Consequently, the knowledge of the differential effective light-path's length (i.e., L_{NO_2}) is crucial to derive the near-surface NO₂ concentrations. The oxygen collisional complex (O₄) can be used as a tracer for the effective light-path in the atmosphere: as its concentration is well-known (it is the square of O₂ concentration). As a result, observed changes of the O₄ dSCDs can be directly attributed to changes in the light-path due to the presence of particles like aerosols and clouds. L_{O_4} is calculated as follows:

$$240 \quad L_{\text{O}_4} = \frac{\text{dSCD}_{\text{O}_4}}{c_{\text{O}_4}} \quad (2)$$

where c_{O_4} is the typical O₄ concentration at the altitude of the instrument.

However, the direct use of the O₄ light-path length in the NO₂ retrieval is not possible under moderate to high pollution conditions, such as those in Brussels, because the profile shapes of O₄ and NO₂ are not the same. In Dimitropoulou et al. (2020), we used radiative transfer model (RTM) simulations to estimate a unitless correction factor, which accounts for these profile shape differences. This unitless correction factor indicates that under moderate to high pollution conditions, L_{NO_2} is equal to or smaller than L_{O_4} . For a correction factor equal or close to one, L_{O_4} is equal to L_{NO_2} , which means that there is a moderate to high aerosol load in the atmosphere during the measurement. On the other hand, correction factors smaller than unity are obtained for measurements performed under aerosol-free conditions or a thin MLH. Assuming a homogeneous NO₂ distribution inside the MLH, the MLH is derived from the NO₂ vertical profiles in the main azimuthal direction and is defined as the ratio of the NO₂ VCD to the near-surface concentration of NO₂. For more information, we refer the reader to Dimitropoulou et al. (2020). The RTM simulations are performed for eight different MLH values of aerosols and NO₂ in the range of 500-2000 m (i.e. eight different combinations) and for different measurement viewing geometries (Solar Zenith Angle



(SZA), Relative Azimuth Angle (RAA) and the corresponding elevation angle of 2°). For every MAX-DOAS measurement, one value of the correction factor is given according to its viewing geometry and MLH value during the measurement.

In the present study, a new dual-scan NO_2 MAX-DOAS retrieval method, which is more suitable for interpreting multi-wavelength measurements than the previous approach (Dimitropoulou et al., 2020), is developed. It is presented in detail in the following subsection.

4.2.1 Developed dual-scan MAX-DOAS retrieval method

The main advantages of the new dual-scan NO_2 MAX-DOAS retrieval method (which are also the main differences with respect to Dimitropoulou et al., 2020) are the following: (1) the direct use of the measured O_4 dSCDs to estimate L_{NO_2} for every measurement, (2) retrieval of near-surface aerosol extinction close to the ground, and (3) the exploitation of the wavelength dependency of the horizontal path representative of MAX-DOAS measurements for the retrieval of the horizontal distribution of aerosols (and therefore NO_2) around the measurement site. The latter is done using O_4 and NO_2 dSCDs measured at six different wavelengths. This new method is described below.

Assuming that the NO_2 vertical distribution can be approximated by a box profile of height equal to mixing layer height (MLH_{NO_2}), the following equation can be used:

$$c_{\text{NO}_2} = \frac{\text{VCD}_{\text{NO}_2}}{\text{MLH}_{\text{NO}_2}} = \frac{\text{dSCD}_{\text{NO}_2}}{L_{\text{NO}_2}} \quad (3)$$

This means that the NO_2 near-surface concentration can be expressed as a ratio of the $\text{dSCD}_{\text{NO}_2}$ to the L_{NO_2} (see Eq. 1) or as a ratio of the VCD_{NO_2} to the MLH_{NO_2} . Using this equation, L_{NO_2} can be estimated as follows:

$$L_{\text{NO}_2} = \text{dSCD}_{\text{NO}_2 \text{ simulated}} \cdot \frac{\text{MLH}_{\text{NO}_2}}{\text{VCD}_{\text{NO}_2}} \quad (4)$$

Here, O_4 dSCDs and L_{NO_2} are simulated using the radiative transfer model VLIDORT version 2.7 (Spurr, 2006). Seasonal median MAX-DOAS NO_2 vertical profiles, as retrieved by applying the MMF inversion algorithm in the main azimuthal direction (see Sect. 4.1), show that the bulk (70 %) of the NO_2 concentration is located inside the MLH_{NO_2} , which is expected since MLH_{NO_2} is estimated as the ratio of VCD_{NO_2} to the near-surface NO_2 concentration. On the other hand, this is not the case for aerosols (only 30 % of the aerosol content is seen to be located inside the MLH_{NO_2}). Considering this feature, for the VLIDORT simulations, the NO_2 a priori profiles are modeled as box profiles with a constant concentration equal to 1.5×10^{11} molec/cm³ from the surface to the MLH_{NO_2} . Two layers compose the aerosol a priori profiles: (1) the MLH_{NO_2} and (2) the free troposphere. The equation, which is applied to estimate the aerosol extinction profile $a(z)$, is the following (see Wang et al., 2014):



$$285 \quad a(z) = \text{AOD} \frac{p}{\text{MLH}_{\text{NO}_2}}, \text{ for } z \leq \text{MLH}_{\text{NO}_2} \quad (5a)$$

and,

$$a(z) = b(\xi, \text{MLH}_{\text{NO}_2}, p) \exp\left(-\frac{z}{\xi}\right), \text{ for } z > \text{MLH}_{\text{NO}_2} \quad (5b)$$

where AOD is the aerosol optical depth, p is the fraction of AOD inside the MLH_{NO_2} , b is a normalizing constant for the exponential component (see Eq. 5 from Wang et al., 2014), z is the simulation altitude grid, and ξ is the scaling height for the aerosols located outside the MLH_{NO_2} , which is set to 5 km (Wang et al., 2014). In the present study, the fraction of AOD located within the MLH_{NO_2} is set to $p=0.3$ (see above). The effect of the p value and the NO_2 profile shape on the retrieved NO_2 near-surface VMRs and VCDs were investigated and considered in the error budget (see Sect. 4.2.2).

The MLH_{NO_2} is estimated per measurement scan, as the ratio of VCD_{NO_2} to the NO_2 near-surface concentration as retrieved in the main azimuthal direction by the MMF inversion algorithm.

295 The RTM simulations have in total nine input parameters, which are the elevation angle, SZA, RAA, AOD, MLH_{NO_2} , c_{NO_2} , AOD (p and ξ), and wavelength. It should be noted that the elevation angle is kept constant (i.e., 2°). For the six different wavelengths (343 nm, 360 nm, 380 nm, 447 nm, 477 nm, and 530 nm), we separately perform RTM simulations and L_{NO_2} (see Eq. 4) are calculated for the assumed SZA, RAA, MLH_{NO_2} , c_{NO_2} , and AOD input scenarios presented in Table 2.

300 **Table 2. RTM inputs for the simulations of L_{NO_2} at the six selected wavelengths (343 nm, 360 nm, 380 nm, 447 nm, 477 nm, and 530 nm).**

| Parameter | Values |
|--|--|
| Wavelength/ nm | 343, 360, 380, 447, 477, 530 |
| SZA/ ° | 20, 30, 40, 50, 60, 70, 80 |
| RAA/ ° | 0, 10, 20, 30, 40, 50, 60, 90, 120, 150, 180 |
| AOD | 0, 0.1, 0.3, 0.4, 0.6, 0.8, 1 |
| p of AOD | 0.30 |
| ξ of AOD/ km | 5 |
| asymmetry parameter | 0.68 |
| Single Scattering Albedo (SSA) | 0.92 |
| MLH/ m | 500, 1000, 1500 |
| Elevation angle/ ° | 2 |
| c_{NO_2} / molec.cm ⁻³ | 1.5×10^{11} |



The O_4 dSCDs are a function of the input parameter AOD. The relation between the simulated O_4 dSCDs and the input AOD values is shown in Fig. 4. A Piecewise cubic hermite interpolating polynomial fitting through the AOD as a function of the simulated O_4 dSCDs for each SZA, RAA, and MLH_{NO_2} combination can be used in order to perform an inverse method (i.e. to estimate the near-surface aerosol extinction from the measured O_4 dSCDs).

For every combination of all eight parameters (i.e., all the parameters of Table 2, except the AOD values), a polynomial fit of L_{NO_2} as a function of simulated O_4 dSCDs is applied. Fig. 5 shows simulated L_{NO_2} as a function of simulated O_4 dSCDs, and a second-order polynomial is fitted through the data points. Since NO_2 is an optically thin absorber, L_{NO_2} is not a function of c_{NO_2} and consequently, a L_{NO_2} value can be estimated for each measurement. Based on the corresponding SZA, RAA, measured O_4 dSCD, and MLH_{NO_2} , a L_{NO_2} is attributed to each low elevation MAX-DOAS measurement through this polynomial fit. To express L_{NO_2} as a function of four different parameters (i.e., O_4 dSCD, SZA, RAA, and MLH_{NO_2}), L_{NO_2} is interpolated linearly at the O_4 dSCD, SZA, RAA, and MLH_{NO_2} of each measurement. For example, a MAX-DOAS measurement with $SZA=30^\circ$, $RAA=60^\circ$, $MLH_{NO_2}=1$ km, and measured O_4 dSCD= 6.10^{43} molec 2 .cm $^{-5}$ will have a L_{NO_2} equal to 15 km at 477 nm (see Fig. 6). Based on this approach, the near-surface NO_2 concentration can be calculated at the six different wavelengths by using Eq. (1) and the derived L_{NO_2} values. The corresponding near-surface NO_2 VMR are obtained by dividing the NO_2 concentrations by the air number density. To derive the air number density, we use monthly averaged pressure and temperature profiles over a 20-year period. These profiles are extracted from the European Centre for Medium-Range Weather Forecasts (ECMWF) ERA-Interim reanalysis. In the last step, the tropospheric NO_2 VCD is calculated from the product of the near-surface NO_2 concentration with the MLH_{NO_2} .

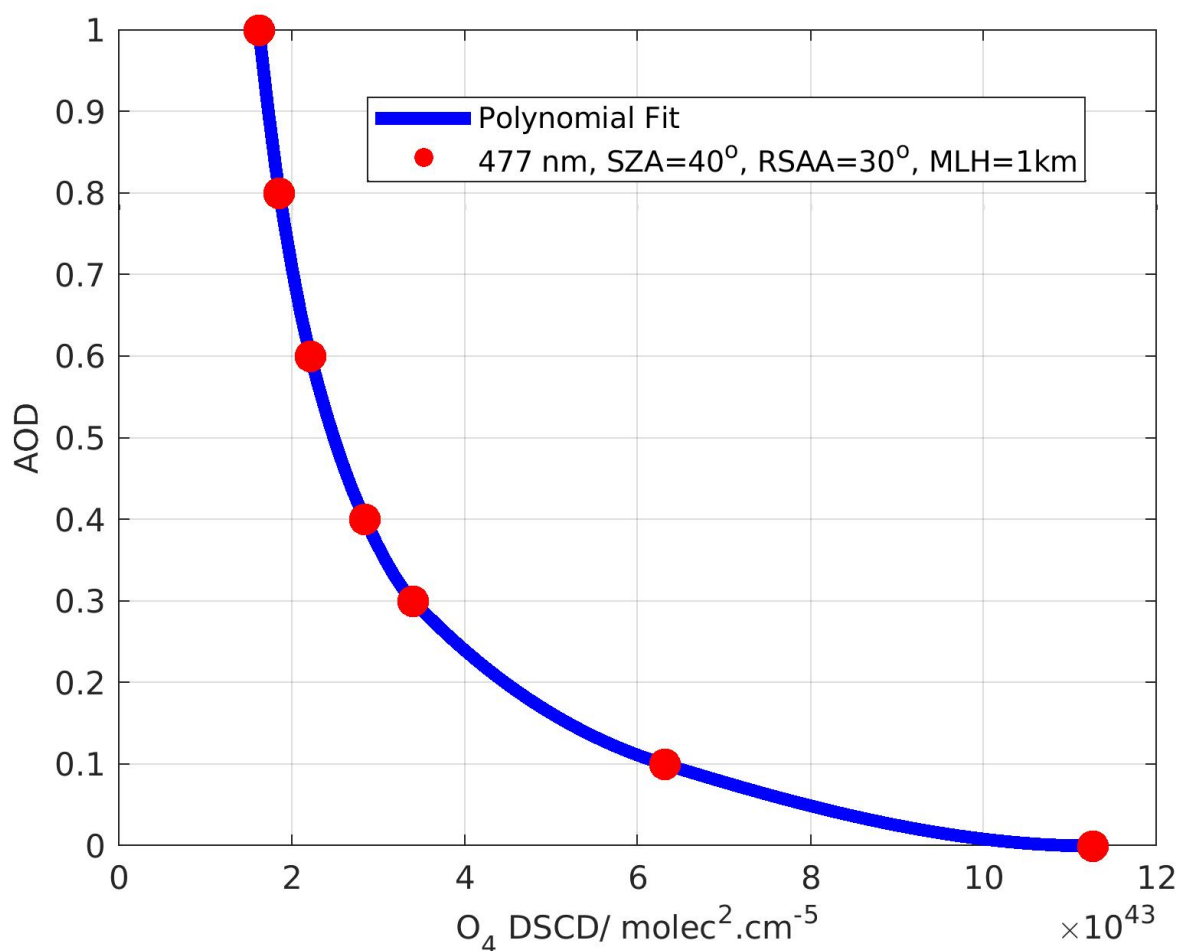
Regarding the aerosols, the AOD is estimated for every off-axis measurement (see Fig. 4). The near-surface aerosol extinction is then calculated as the ratio between the aerosols inside the MLH_{NO_2} (i.e., AOD times p) and MLH_{NO_2} . The near-surface aerosol extinction refers to the layer that extends from the surface to the MLH_{NO_2} . As discussed above, around 30% of the total aerosols is expected to be found inside this layer.

The effect of SZA, RAA, and MLH_{NO_2} on the simulated L_{NO_2} is investigated in the supplement. First, the simulated L_{NO_2} are presented in Fig. S1 as a function of RAA for different MLH_{NO_2} and wavelengths and a single AOD and SZA value. L_{NO_2} strongly depends on MLH_{NO_2} . The lower the MLH_{NO_2} , the shorter the L_{NO_2} is. The same NO_2 concentration and aerosol load are used for the three different MLH_{NO_2} scenarios. So, when aerosols are concentrated in a thin layer (i.e., $MLH_{NO_2}=0.5$ km), L_{NO_2} becomes shorter. Secondly, we observe that L_{NO_2} depends on RAA. The larger the RAA, the longer the L_{NO_2} . In Fig. S2, simulated L_{NO_2} are plotted for each wavelength and each considered MLH_{NO_2} as a function of SZA (at a constant AOD and RAA). L_{NO_2} depends strongly on SZA. The highest dependency is observed for large SZA values, where L_{NO_2} becomes maximum. Finally, in both Fig. S1 and S2, we observe that L_{NO_2} becomes longer with wavelength, which is expected because of the less pronounced Rayleigh scattering at longer wavelengths.

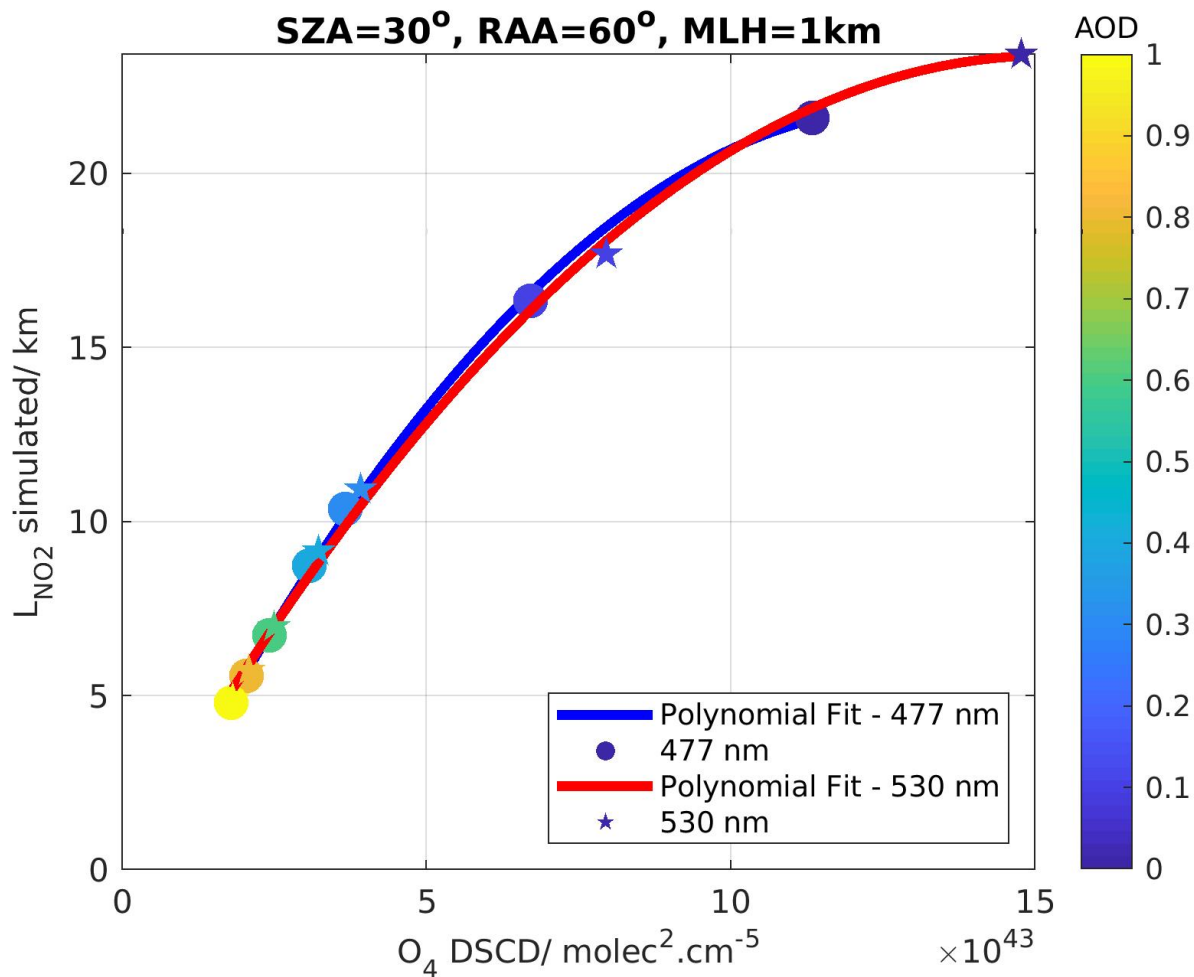


An example of dual-scan MAX-DOAS retrieval is shown in Fig. 6. Based on the RTM simulations described above, L_{NO_2} is derived for the wavelengths of interest, and ultimately, near-surface NO_2 concentrations and tropospheric NO_2 VCDs are estimated. In the last step, the near-surface aerosol extinction values are assigned to the six different wavelengths.

340



345 **Figure 4. Dots: Simulated AOD for NO_2 box profile of 1 km at 477nm for a SZA of 40° and RAA of 30° as a function of the simulated O_4 DSCDs for the different AOD values (1, 0.8, 0.6, 0.4, 0.3, 0.1 and 0; see Table 2). Blue line: simulated AOD by applying an exponential fit through the data points.**



350

Figure 5. Dots (stars): Simulated L_{NO_2} for NO_2 box profile of 1 km at 477nm (530 nm) for a SZA of 30° and RAA of 60° as a function of the simulated O_4 DSCDs for the different AOD values (1, 0.8, 0.6, 0.4, 0.3, 0.1 and 0; see Table 2). Blue (red) line: 2nd-order polynomial fit through the data points.

355

360

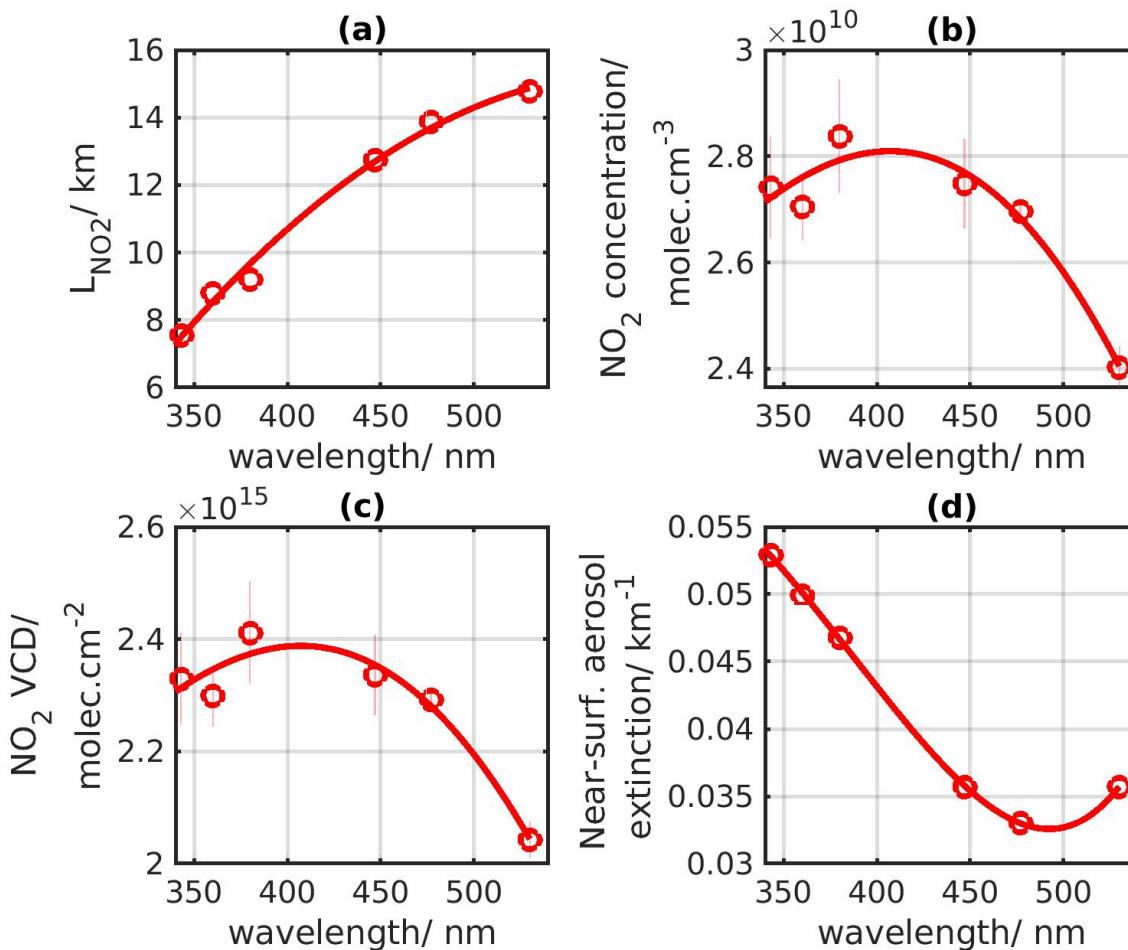


Figure 6. (a) Corresponding L_{NO_2} , (b) near-surface NO_2 concentrations, (c) NO_2 VCDs, and (d) aerosol optical densities as a function of the six wavelengths used in the retrieval (11 September 2018, 11:51 UTC, 123.5° azimuthal direction).

365

4.2.2 Uncertainty budget

To estimate uncertainties on the dual-scan parameterized NO_2 near-surface concentration and VCD, the standard error propagation method is used as:

$$370 \quad \sigma_{c_{NO_2}}^2 = \left(\sigma_{dSCD_{NO_2}} \frac{\partial c_{NO_2}}{\partial dSCD_{NO_2}} \right)^2 + \left(\sigma_{L_{NO_2}} \frac{\partial c_{NO_2}}{\partial L_{NO_2}} \right)^2 \quad (6)$$

which is solved as:



$$\sigma_{c_{NO_2}}^2 = \left(\sigma_{dSCD_{NO_2}} \frac{c_{NO_2}}{dSCD_{NO_2}} \right)^2 + \left(\sigma_{L_{NO_2}} \frac{c_{NO_2}}{L_{NO_2}} \right)^2 \quad (7)$$

According to Kreher et al. (2019) and Bösch et al. (2018), in urban or suburban polluted conditions, the use of the DOAS fit
375 uncertainty of NO₂ for the dSCD_{NO₂} uncertainty is not appropriate, because the dSCD_{NO₂} uncertainty is mostly driven by
atmospheric variability as well as spatial and temporal fluctuations in the O₄ and NO₂ fields. In this study, a conservative value
of 3.5x10¹⁵ molec.cm⁻² is attributed to $\sigma_{dSCD_{NO_2}}$ (Kreher et al., 2019). This represents an error of up to 5% on the NO₂ dSCDs
in the visible range (477 nm).

The second error source is related to the estimation of L_{NO₂} from the RTM simulations. To estimate this error, sensitivity tests
380 on the input aerosol and NO₂ vertical profiles were performed. The fraction of aerosols located inside the MLH_{NO₂} (40% and
60% instead of 30%) and the NO₂ profile shape (linearly decreasing instead of box) were modified. The error related to the
RTM simulations is about 11% in the Visible range (477 nm).

Combining all the error sources, the total uncertainties on the NO₂ near-surface concentration is about 16%, 15%, 14%, 11%,
10%, and 10% in 343 nm, 360 nm, 380 nm, 447 nm, 477 nm, and 530 nm, respectively.

385 The NO₂ VCD is the product of the NO₂ near-surface concentration and MLH_{NO₂}. According to Dimitropoulou et al. (2020),
the uncertainty related to MLH_{NO₂} is about 4%. It is found that the relative difference between MLH_{NO₂} values derived in the
main azimuthal directions and in other three additional directions depends strongly from the direction (see Section 4.2.3). In a
refined version, this direction dependent error source on the NO₂ near-surface concentration will be included in the uncertainty
budget.

390 By using this finding, the total uncertainties on the NO₂ VCD is about 17%, 16%, 15%, 11%, 11%, and 10% in 343 nm, 360
nm, 380 nm, 447 nm, 477 nm, and 530 nm, respectively.

4.2.3 Validation of the dual-scan MAX-DOAS retrieval method

The sanity check and validation of the dual-scan MAX-DOAS retrieval method in Uccle is based on two different correlative
395 comparisons.

The sanity check compares the NO₂ near-surface VMRs and tropospheric VCDs retrieved by the dual-scan parameterization
in the main azimuthal direction to the same quantities retrieved with the MMF inversion algorithm at the two main wavelengths
(360 nm and 477 nm). As can be seen in Figures 7 and 8, both data sets are in good agreement, with correlation coefficient
values in the range of 0.86 to 0.95 and slope values close to unity for all the four comparisons.

400 The validation step is based on the same type of comparison as the first one but for three additional azimuthal directions, where
elevation scans, and hence profile retrievals, are available for some periods. Onward July 3, 2019, elevation scans were
performed in these three additional azimuthal directions to complement the already existing measurement set-up. These
elevation scans were performed once per day, around noon, in the 11°, 105°, and 262.5° azimuthal directions. Figure 9 shows



the comparison between near-surface NO₂ VMRs and tropospheric VCDs retrieved by the dual-scan parameterization method
405 and the corresponding results obtained with the MMF inversion algorithm. Overall good agreement is obtained ($R=0.79$ and
0.84 for near-surface VMR and VCD, respectively). We observe that the comparison concerning the near-surface NO₂ VMR
seems to be noisier than in the main azimuth direction. This is mainly due to the use of the MLH_{NO_2} calculated in the main
azimuthal direction for all the different azimuth angles in the dual-scan method. Additionally, the parameterization technique
slightly underestimated the near-surface NO₂ VMR ($s=0.84$) while a slope value of 1.00 is obtained for tropospheric VCDs.
410

415

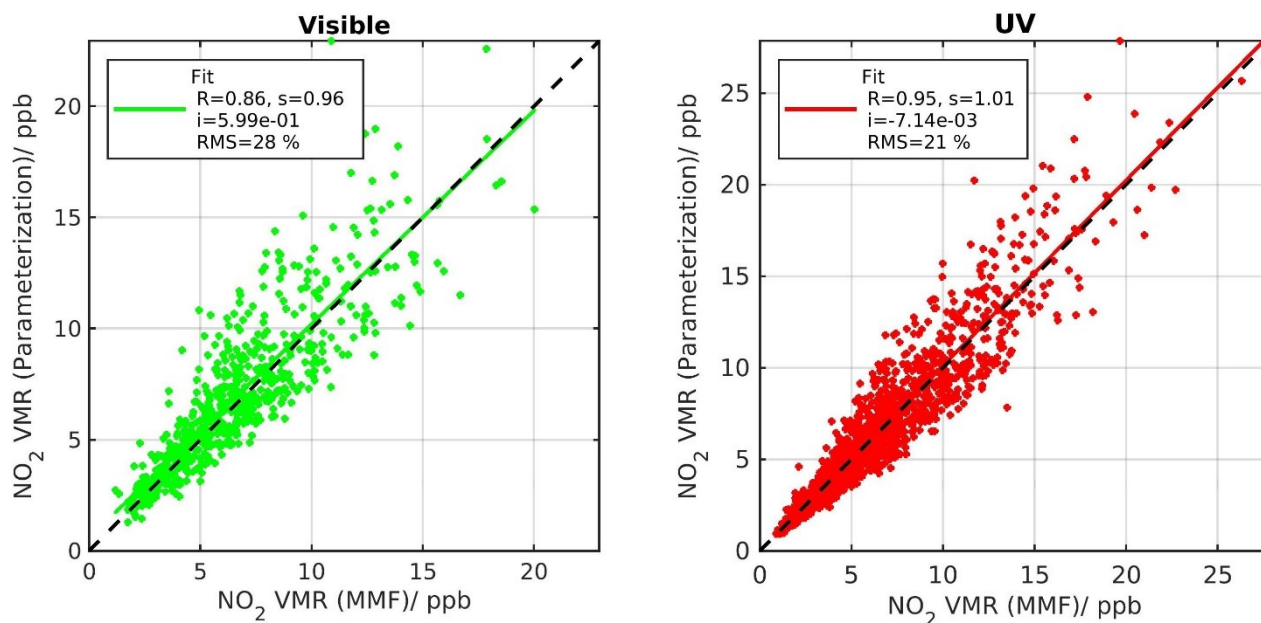
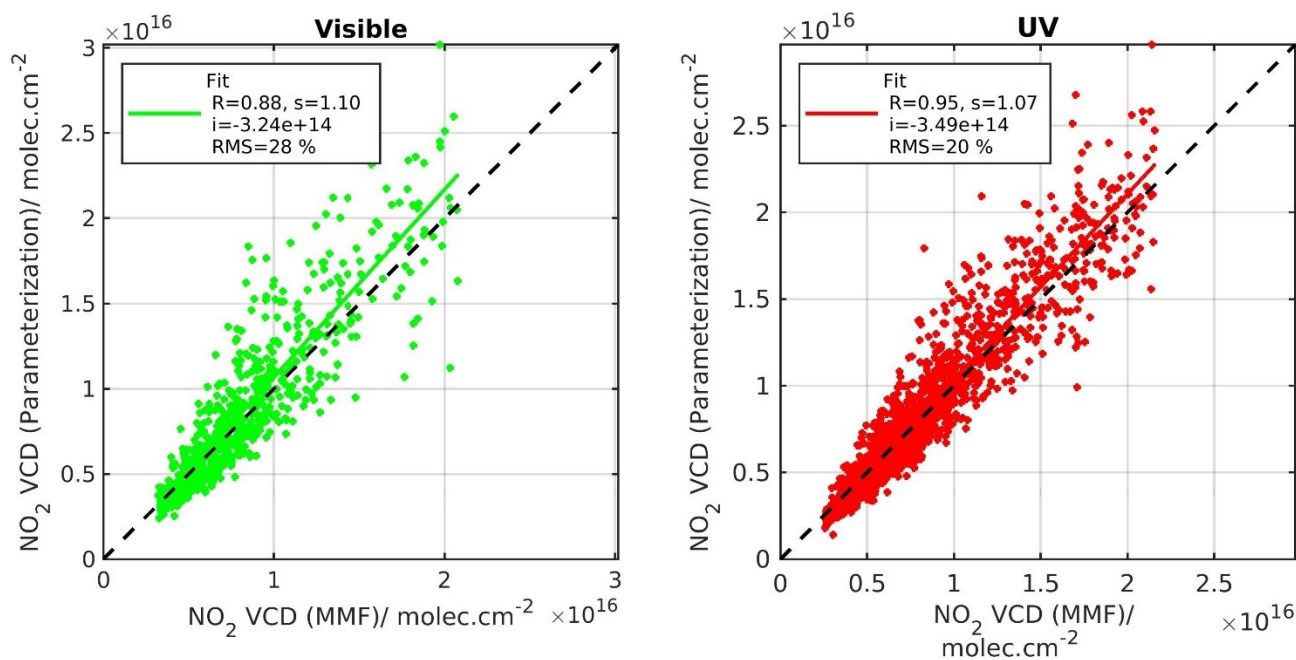


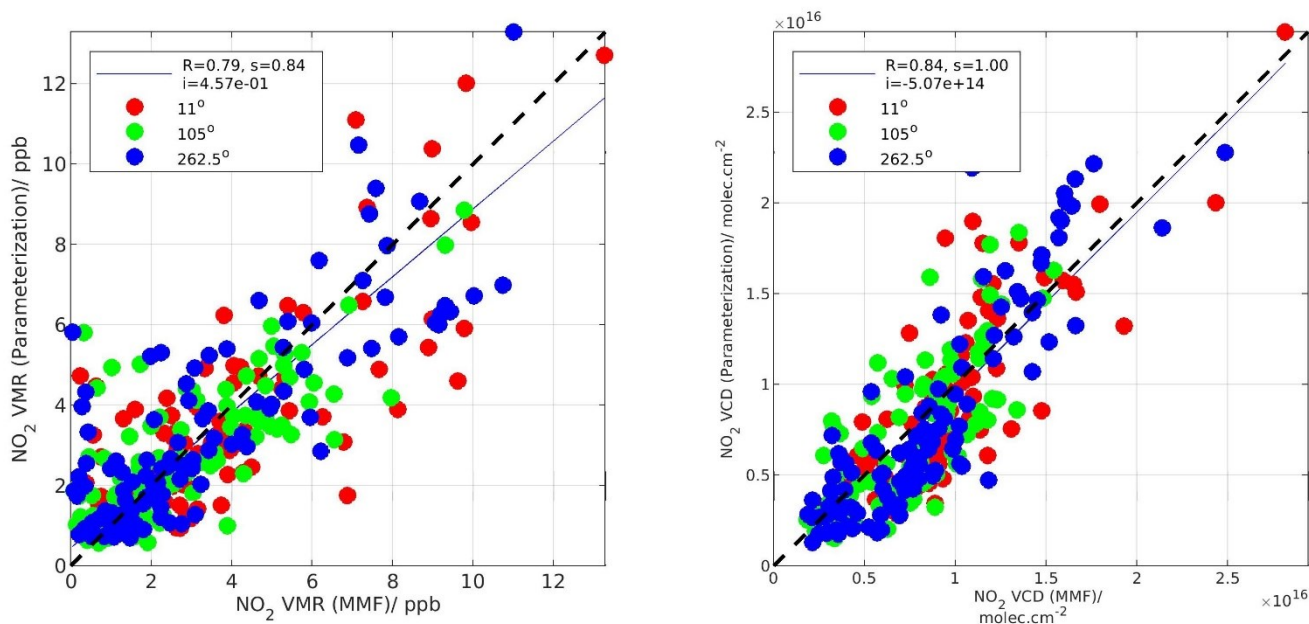
Figure 7. Comparison between MMF and parameterized NO₂ near-surface VMR at 477 nm (Visible, left panel), and 360 nm (UV, right panel), as derived from the main azimuthal direction (i.e., 35.5° azimuthal direction).

420



425 **Figure 8.** Comparison between MMF and parameterized NO₂ VCD at 477 nm (Visible, left panel), and 360 nm (UV,
right panel), as derived from the main azimuthal direction (i.e., 35.5° azimuthal direction).

430



435 **Figure 9. Visible range: comparison between MMF and (left panel) parameterized NO₂ near-surface VMR and (right**
panel) parameterized NO₂ VCD at three different azimuthal directions, as indicated in the color bar (11°, 105°, and
262.5° azimuthal directions). The elevation scans in these azimuthal directions were performed once per day from 3
July 2019.

4.3 Horizontal distribution inversion approach

440 The parameterized NO₂ near-surface concentrations at the six different wavelengths are used as input in a new horizontal
distribution inversion approach. As parameterized NO₂ near-surface concentrations, we refer to the conversion of the measured
NO₂ dSCDs (i.e. at the elevation angle of 2°) to near-surface NO₂ concentrations by applying the dual-scan MAX-DOAS
retrieval method as described in Sect. 4.2. Figure 10 shows a sketch of the assumed horizontal box model configuration, in
which successive boxes of concentration c_N between the horizontal distances x_{N-1} and x_N from the MAX-DOAS instrument are
considered along the light path. The index N is equal to the total number of successive boxes.

445 The different horizontal lines illustrate the horizontal extent (or differential effective light path as described in Sect. 4.2) in
which the NO₂ near-surface concentrations are extended for the six different wavelengths. Generally, the MAX-DOAS
horizontal sensitivities are longer for larger wavelengths because of the less pronounced Rayleigh scattering (see also Fig. 6;
Ortega et al., 2016; Dimitropoulou et al., 2020). In Fig. 10, the shortest line represents the smallest wavelength's horizontal



sensitivity (343 nm), and the longest line the largest wavelength's horizontal sensitivity (530 nm). As can be seen in the sketch,
 450 the effective horizontal light path at the six different wavelengths passes through different number of horizontal bins.

The parameterized NO₂ near-surface concentrations at the different wavelengths are the mean concentrations along the
 horizontal effective light paths (see Section 4.2), which are also called differential effective light paths because they are linked
 to the dSCD_{NO₂}. When having information coming from one wavelength only, it is not possible to know how the NO₂ is
 distributed along this light path. In the present work, the knowledge of mean NO₂ concentrations at six different wavelengths
 455 is used to retrieve a horizontal NO₂ profile, assuming the horizontal box model described in Fig. 10. This new retrieval method
 is described below.

The measurement vector \mathbf{y} consists of the six retrieved surface concentrations (called as \bar{c}_{NO_2} ; see method presented in Sect.
 4.2) at the six different wavelengths. These near-surface concentrations can be expressed as functions of the different effective
 460 light paths (L_{NO_2}) and correspond to the average surface concentrations along those L_{NO_2} :

$$\mathbf{y} = \mathbf{F}_{\text{meas}}(\mathbf{c}_{\text{NO}_2, \text{true}}) = \bar{c}_{\text{NO}_2} = \frac{\text{dSCD}_{\text{NO}_2}}{L_{\text{NO}_2}} \quad (8)$$

$\mathbf{F}_{\text{calcul}}$, which represents the forward model, can be expressed as follows:
 465

$$\mathbf{F}_{\text{calcul}}(\mathbf{c}_{\text{NO}_2, \text{true}}) = \frac{1}{L_{\text{NO}_2}} \int_0^{L_{\text{NO}_2}} \mathbf{c}_{\text{NO}_2}(x) dx \quad (9)$$

where x is the horizontal distance and \mathbf{c}_{NO_2} the NO₂ near-surface concentration as a function of x , the distance from the MAX-
 DOAS instrument.

470 Our retrieval of the horizontal distribution of \mathbf{c}_{NO_2} is based on the inversion theory (Rodgers, 2000), in which a horizontal
 profile \mathbf{c}_{NO_2} (state vector) is retrieved given an a-priori horizontal profile \mathbf{x}_a , the measurement vector \mathbf{y} , the matrix of the
 weighting function \mathbf{K} , the uncertainty covariance matrix of the a priori \mathbf{S}_a and the uncertainty covariance matrix of the
 measurement \mathbf{S}_e :

$$475 \quad \mathbf{c}_{\text{NO}_2} = \mathbf{x}_a + (\mathbf{K}^T \mathbf{S}_e^{-1} \mathbf{K} + \mathbf{S}_a^{-1})^{-1} \mathbf{K}^T \mathbf{S}_e^{-1} (\mathbf{y} - \mathbf{K} \mathbf{x}_a) \quad (10)$$

The weighting function indicates the sensitivity of the measurement vector to a change in the horizontal profile. It is given in
 the present case by the following analytical functions:



$$\mathbf{K}(x, L_{\text{NO}_2}) = \frac{dF_{\text{calcul}}}{dc_{\text{NO}_2}} = \begin{cases} \frac{dx}{L_{\text{NO}_2}} & \text{for } 0 < x < L_{\text{NO}_2} \\ A \frac{dx}{L_{\text{NO}_2}} & \text{for } x \text{ (last)} > L_{\text{NO}_2} \\ \mathbf{0} & \text{for } x > L_{\text{NO}_2} \end{cases} \quad (11)$$

480

where A is the coverage percentage of the differential effective light path length at the last horizontal grid.

An example of weighting functions is presented in Fig. 11. As can be seen, each measurement is sensitive from the MAX-DOAS instrument location to the horizontal distance equal to the differential effective light path length of each measurement. As each last horizontal grid is not fully covered by each measurement, the coverage percentage is considered for these grid
485 cells. It should be noted that since NO_2 is an optically thin absorber, the measurements depend linearly on each horizontal box's concentration. For this reason, OEM for the linear case is considered here, and only one inversion step is needed (see Eq. 10).

The selected output horizontal grid for the retrieval extends from the MAX-DOAS instrument to the maximum differential effective light path (L_{NO_2} at 530 nm) per azimuthal direction and consists of successive boxes of 0.5 km thickness on the
490 horizontal axis.

Since this inversion problem is ill-conditioned, more than one horizontal NO_2 profile can be consistent with the measurement vector. To reject unrealistic solutions, the a priori profile \mathbf{x}_a and its uncertainty covariance matrix must be included in the retrieval. In the OEM, the a priori information usually comes from an independent source, like a model or other correlative measurements. In the present study, RIO model data were chosen as a priori. RIO is a land-use regression model based on the
495 interpolation of the hourly NO_2 near-surface concentrations measured by the in-situ telemetric air quality network in Belgium (Hooyberghs et al., 2006; Janssen et al., 2008). RIO provides hourly NO_2 concentration maps on a $4 \times 4 \text{ km}^2$ spatial resolution. Seasonal average maps of RIO NO_2 near-surface concentration are constructed (see Fig. S3) and after, seasonal averages of RIO NO_2 near-surface concentration horizontal profiles were calculated in each azimuthal direction and interpolated on the retrieval's horizontal grid by regriding the initial $4 \times 4 \text{ km}^2$ spatial resolution to a finer one (see Fig. 12). The shape of the RIO
500 a priori NO_2 profiles per azimuthal direction stays the same during different seasons of the year, indicating that the wind effect on NO_2 transportation disappears by the seasonal averaging and that the same sources contribute to the NO_2 horizontal field. A mean scaling factor equal to the mean ratio between the measured and RIO NO_2 near-surface concentrations is applied because of the systematic underestimation of NO_2 near-surface concentrations by MAX-DOAS when compared to in-situ measurements (Dimitropoulou et al., 2020).

505 For the aerosols horizontal distribution retrieval, there are not sufficient independent measurements that provide information about the horizontal distribution of AOD and can serve as an a priori AOD profile. Therefore, a horizontally constant a priori AOD profile is used in the AOD retrieval based on CIMEL observations. An AOD equal to 0.18, which is the yearly-averaged AOD value from CIMEL at 477 nm, is used. To construct the near-surface aerosol extinction a priori profiles, it is considered



that 30% of the total amount of AOD is located inside the MLH (i.e., known for each MAX-DOAS vertical scan from the
510 MMF inversion algorithm; see Section 4.1).

The diagonal elements of the S_a matrix are set equal to the square of a scaling factor times the NO_2 concentration a priori profile. The non-diagonal elements, which account for correlation between the different horizontal grid cells, are set as follows (Barret et al., 2002):

$$515 \quad S_{a_{ij}} = \sqrt{S_{a_{ii}} S_{a_{jj}} \exp\left(-\ln(2) \left(\frac{x_i - x_j}{\gamma}\right)^2\right)} \quad (12)$$

where x_i and x_j are the horizontal distances at the i^{th} , and j^{th} horizontal boxes and γ is half of the correlation length. γ is set equal to 3.5 km. To eliminate inversion instabilities, S_a elements which are smaller than 0.1% of the maximum S_a element are set equal to zero.

520 To estimate the correlation length, a covariance matrix was constructed by exploiting the airborne observations above Brussels (28 June 2019). The airborne observations have a spatial resolution of approximately $100 \times 100 \text{ m}^2$. NO_2 horizontal profiles were constructed in different azimuthal directions in a spatial resolution of $500 \times 500 \text{ m}^2$, expanding from the MAX-DOAS's position to a maximum distance of 20 km, and were used to calculate a covariance matrix. A correlation length equal to 7 km, and consequently, a gamma value equal to 3.5 km, is found to be representative for the NO_2 horizontal profiles in Brussels.

525 Using this correlation length, a variance of 45% is used. This choice was conducted based on the seasonal variance of the RIO a priori profiles compared to their seasonal mean value. It is found that the seasonal variance of RIO observations has a mean value of 45%. Additionally, it is found to be a good compromise for obtaining reasonable retrieval results e.g. in terms of information content, and while avoiding unrealistic oscillations in the retrieved aerosol and NO_2 profiles.

The measurement covariance matrix S_e is chosen to be diagonal, with elements corresponding to the uncertainties of the dual-
530 scan parameterized NO_2 near-surface concentration (see Section 4.2.2).

An example of the retrieved NO_2 horizontal profile is presented in Fig. 13, together with corresponding measured and simulated \bar{c}_{NO_2} at the six different wavelengths for July 2, 2018 (25° azimuthal direction). RMS is calculated between measured and simulated NO_2 near-surface concentrations of the horizontal retrieval normalized by the mean of the measured NO_2 near-surface concentrations (upper panel in Fig. 13). For distances smaller than the minimum L_{NO_2} (around 8 km), the measurements
535 do not give information about the horizontal distribution of NO_2 . Consequently, the retrieved NO_2 horizontal profile at these ranges is coming from the a priori profile. Similarly, the measured and retrieved near-surface aerosol extinction coefficient and the retrieved aerosol horizontal profile are shown in Fig. 14, for one sample case on 11 September 2018 (167.5° azimuthal direction).

An essential condition of the dual-scan MAX-DOAS retrieval and the new horizontal inversion approach at six different
540 wavelengths is the increasing trend of the horizontal sensitivity as a function of wavelength. Consequently, every wavelength is sensitive to a different horizontal region and the six different wavelengths can be used to retrieve the horizontal distribution



of aerosols and trace gases. Sensitivity tests were conducted in which simulated L_{O_4} are expressed as a function of the six different wavelengths for different aerosol conditions. As can be seen in Fig. S4, the linear relationship between L_{O_4} (and L_{NO_2}) and wavelength exists for AOD values ranging from 0 to 1. An AOD equal to unity is chosen as the maximum AOD of the simulations because in Uccle, AOD values rarely exceed one (see in <https://aeronet.gsfc.nasa.gov/> for the Brussels measurement site). Therefore, the relation stays linear as the aerosol load changes for the conditions observed in Uccle. The only condition leading to non-linearity is when clouds are present. However, as explained in Sect. 4.1, a cloud filtering approach is applied, rejecting the broken cloud scenes, which are the more problematic ones.

550

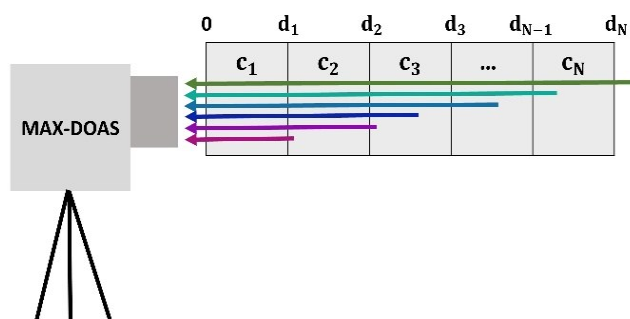
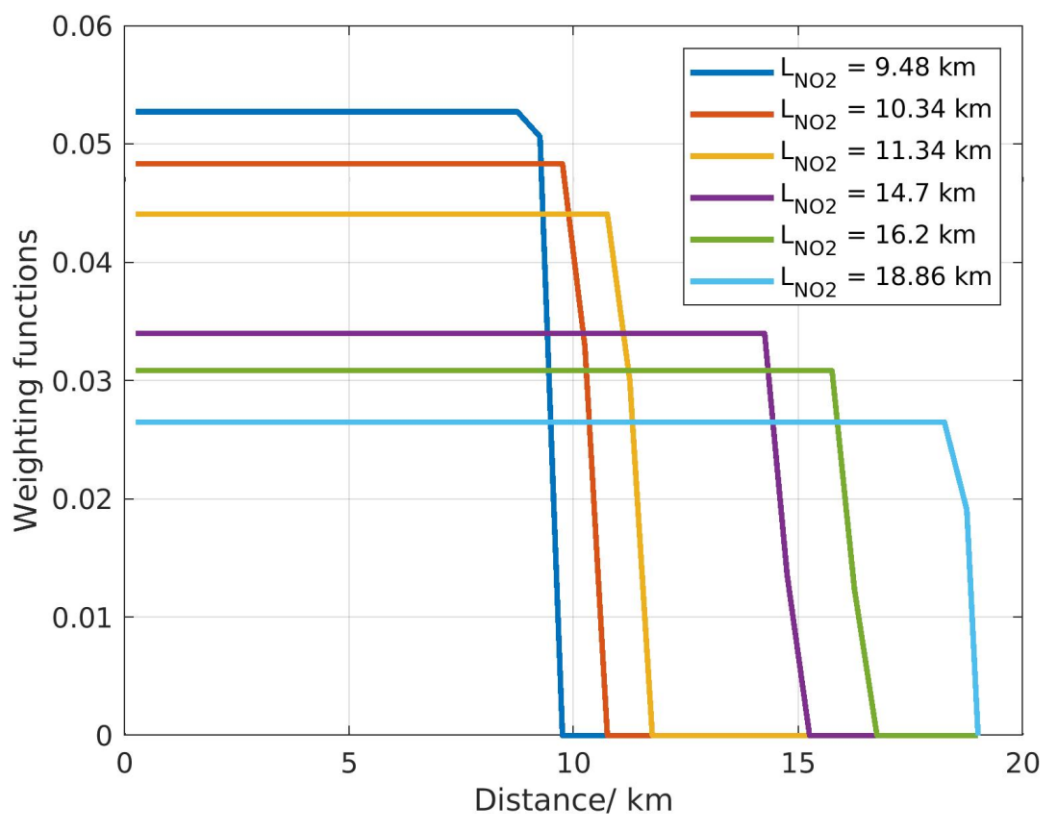


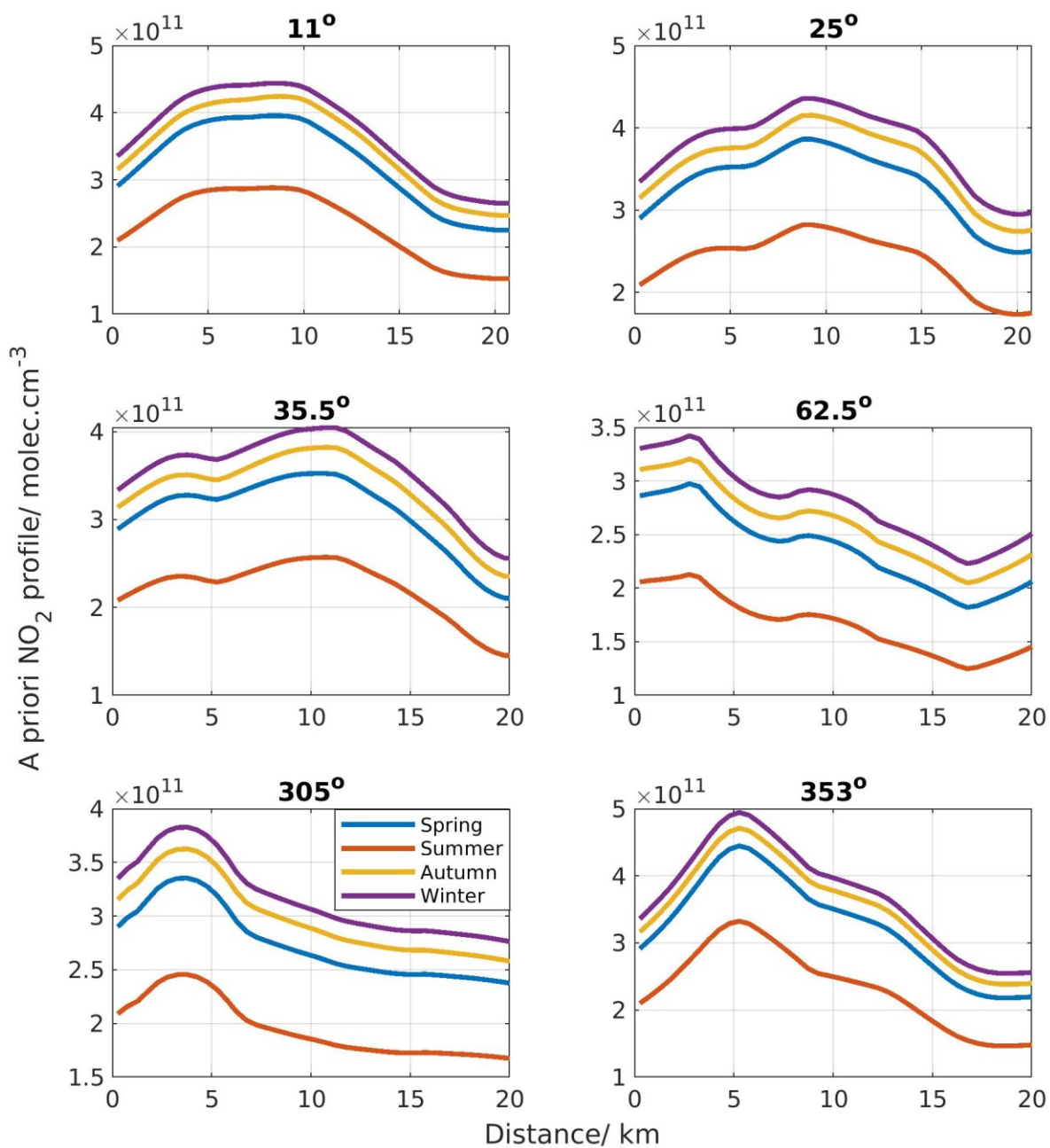
Figure 10. Schematic representation of the six different L_{NO_2} (i.e., one horizontal line for each wavelength) used in the new horizontal distribution inversion approach. The length of each line shows the sensitivity of each wavelength as a function of the horizontal distance. The shortest line represents the smallest wavelength.

555



560 **Figure 11. Examples of weighting functions used in the new horizontal distribution inversion approach (11 September 2018).**

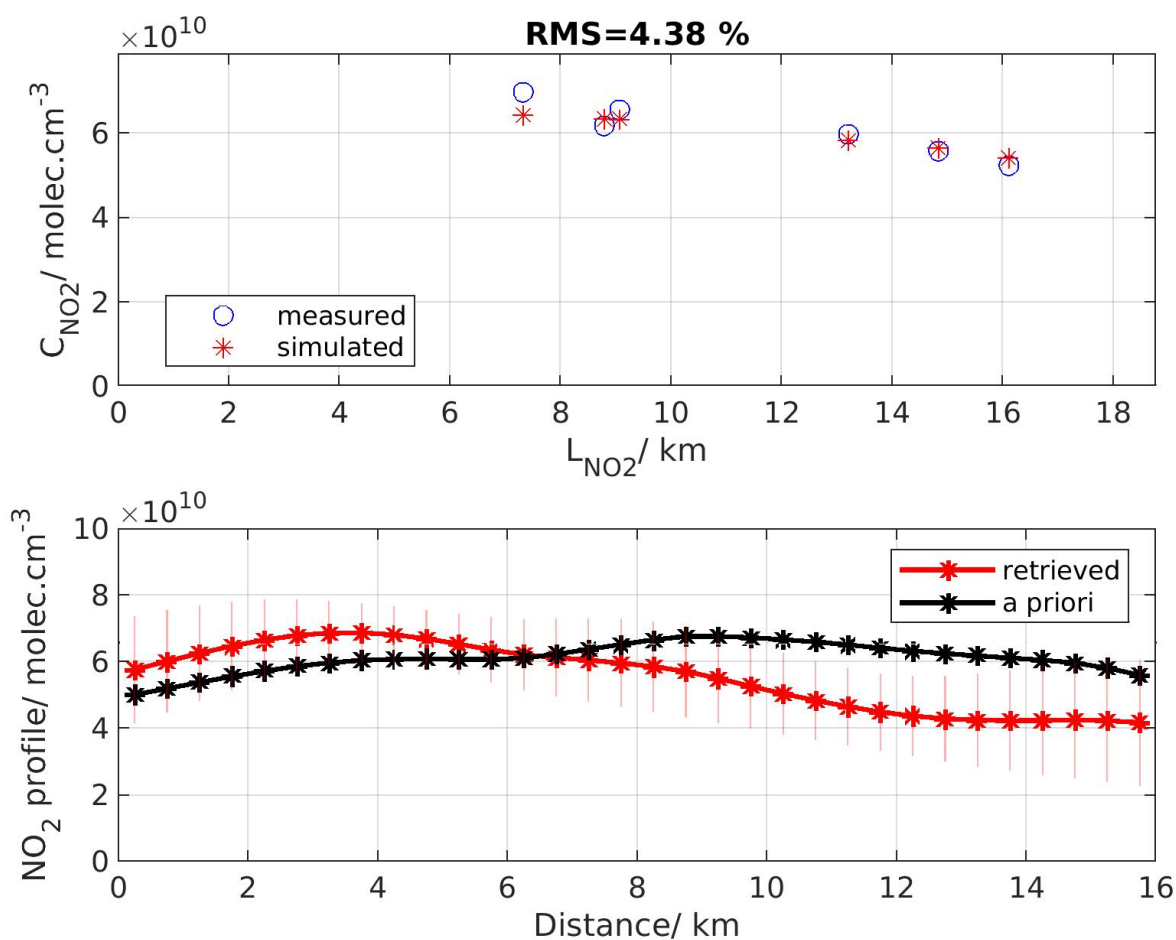
565





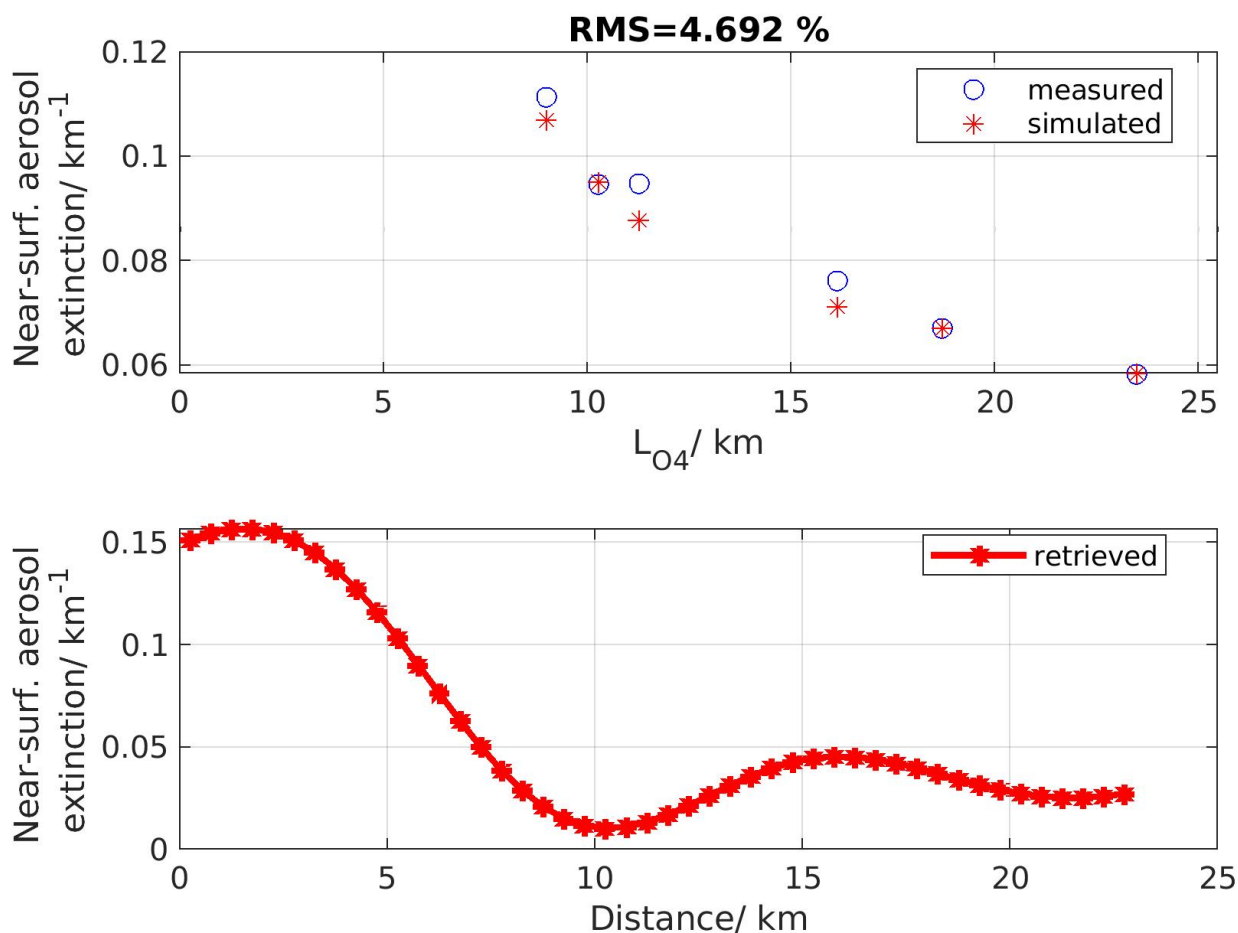
570 **Figure 12. Example of seasonal *a priori* NO₂ horizontal profiles for the new horizontal distribution inversion approach as a function of the horizontal distance from the MAX-DOAS instrument in six different azimuthal viewing directions, before the application of the scaling factor.**

575



580 **Figure 13. (Upper panel) Measured and retrieved NO₂ near-surface concentrations at the six different wavelengths (i.e., horizontal distances) as a function of the estimated horizontal distances and (lower panel) the retrieved NO₂ near-surface horizontal profile and a priori profile (02 July 2018, 10.42 UTC, 25° azimuthal direction).**

580



585 **Figure 14. (Upper panel) Measured and retrieved near-surface aerosol extinction at the six different wavelengths (i.e., horizontal distances) as a function of the estimated horizontal distances and (lower panel) the retrieved near-surface aerosol extinction horizontal profile (11 September 2018, 11.48 UTC, 167.5° azimuthal direction).**

590 4.4 Characterization of the retrieval

To characterize the retrieval, the averaging kernels, **AK**, play a crucial role. The **AK** matrix is calculated as follows (Rodgers, 2000):



$$\mathbf{AK} = \frac{dc_{NO_2}}{dc_{NO_2,true}} = (\mathbf{K}^T \mathbf{S}_e^{-1} \mathbf{K} + \mathbf{S}_a^{-1})^{-1} \mathbf{K}^T \mathbf{S}_e^{-1} \mathbf{K} \quad (13)$$

595

The **AKs** are the rows of the **AK** matrix. They present the sensitivity of the retrieved (c_{NO_2}) on the true ($c_{NO_2,true}$) atmospheric profile. Ideally, the **AK** matrix should be an identity matrix. In Fig. 15, an example of selected **AKs** is shown. As can be seen, for distances smaller than the first measurement (e.g., near-surface NO_2 concentration retrieved at 343 nm), the **AKs** are constantly zero (or have small values) from the MAX-DOAS instrument until these distances. This indicates a low sensitivity on these short distances, and therefore information about the horizontal distribution of NO_2 is coming essentially from the a priori profile. The **AKs** create a maximum flat plateau close their nominal horizontal distance for larger distances ($d=7.25$ km, $d=8.75$ km, and $d=15.75$ km). For this particular example, the **AKs** do not exceed the values of 0.25.

600

Another important information about the retrieval is the trace of the **AK** matrix, which refers to the number of degrees of freedom for signal (DOFS). The DOFS are an indication of the number of independent pieces of information that one can retrieve from the measurements. Ideally, the DOFS would be equal to the number of horizontal boxes for the horizontal distribution. In reality, the DOFS are lower, because of the limited horizontal resolution of the measurements. In Fig. 15, the DOFS are close to three, which means that three independent pieces of information are contained in the measurements for this particular example.

605

610 In the present work, the total retrieval error is equal to the error related to the measurement noise. According to Rodgers (2000), the retrieval noise error is estimated as:

$$\mathbf{S}_{meas} = \mathbf{G} \mathbf{S}_e \mathbf{G}^T \quad (14)$$

with, \mathbf{G} being the gain matrix:

$$\mathbf{G} = (\mathbf{K}^T \mathbf{S}_e^{-1} \mathbf{K} + \mathbf{S}_a^{-1})^{-1} \mathbf{K}^T \mathbf{S}_e^{-1} \quad (15)$$

615

The horizontal profiles of the measurement error in percentage are shown in Fig. 16. As can be seen, the measurement error becomes maximum for the longest distance.

620 To eliminate the unsuccessful retrievals, the percentage of accepted retrievals with respect to the total number of retrievals during the four seasons is investigated when a specific filtering on RMS and DOFS is applied (see Table 3). From these tests, it is found that most of the retrievals have DOFS larger than 1.5. RMS is defined as the root-mean-square deviation between measured and simulated c_{NO_2} normalized by the mean of the measured c_{NO_2} (e.g., same RMS as in Fig.13). Table 3 indicates that most of the retrievals have an RMS smaller than 6% with a median RMS value of around 4.5% during all seasons. Based on these investigations, $DOFS > 1.5$ and $RMS < 6\%$ are used as retrieval quality control criteria.

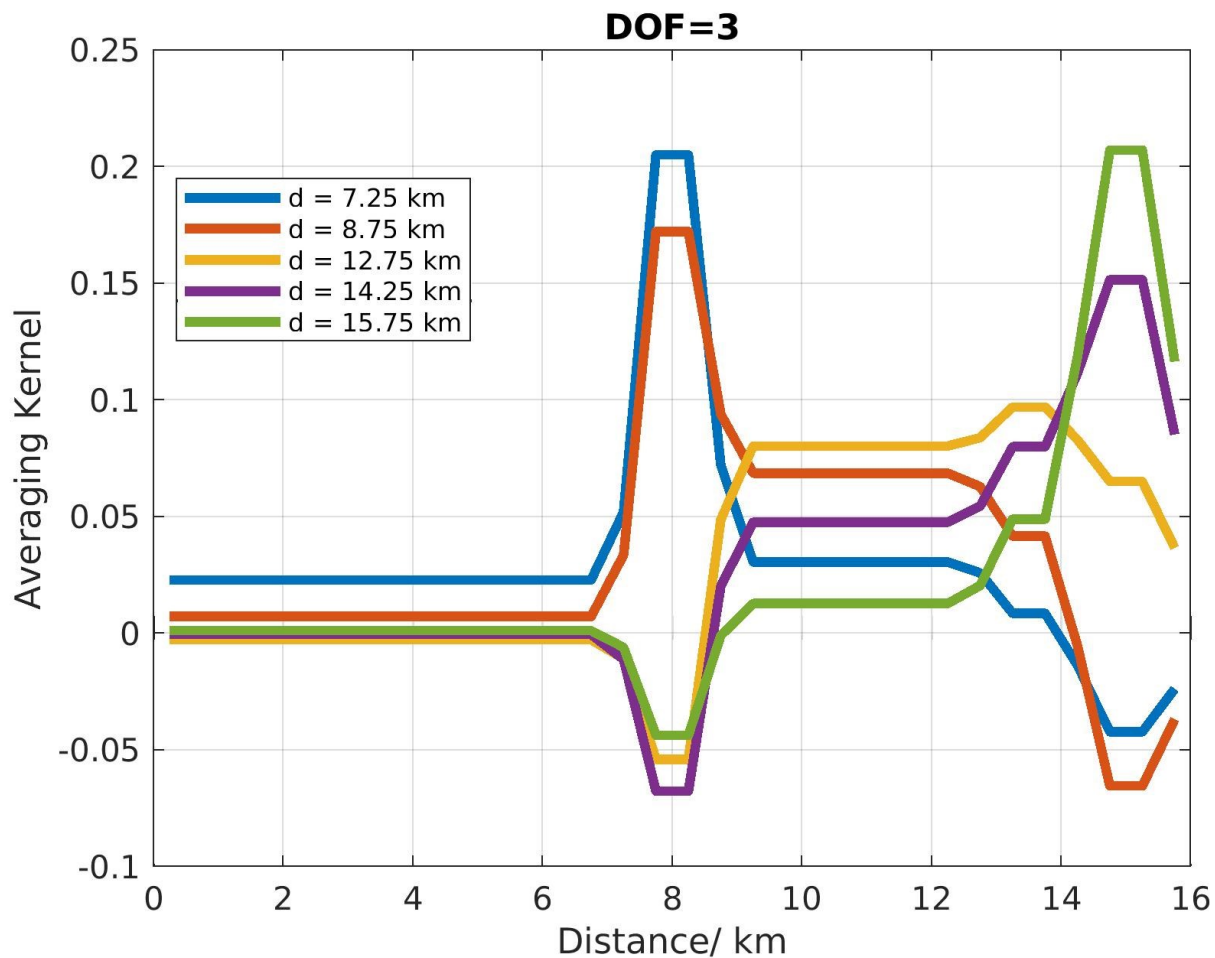
625



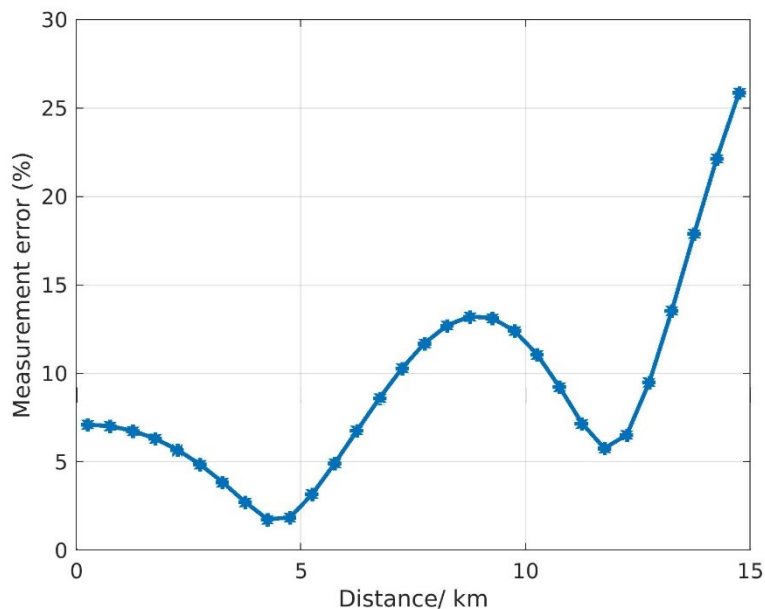
630 **Table 3. Seasonally averaged root-mean-square (RMS) and DOFS values. RMS is calculated between measured and retrieved NO₂ near-surface concentrations of the horizontal retrieval (Fig. 13a). DOFS represent the degrees of freedom of the horizontal retrieval (Fig. 15). The percentage of the accepted retrievals is presented for the different selection criteria.**

| Season | Spring | Summer | Autumn | Winter |
|--|--------|--------|--------|--------|
| Medium RMS (%) | 3.8 | 4.7 | 4.7 | 4.8 |
| Median DOFS | 1.7 | 1.7 | 1.6 | 1.6 |
| Accepted retrievals (%) (DOFS>1.5) | 90 | 91 | 81 | 78 |
| Accepted retrievals (%) (RMS<6%) | 87 | 72 | 70 | 73 |
| Accepted retrievals (%) (RMS<5%) | 75 | 57 | 55 | 55 |
| Accepted retrievals (%) (RMS<4%) | 56 | 33 | 36 | 32 |
| Accepted retrievals (%) (RMS<3%) | 27 | 11 | 15 | 11 |
| Total accepted retrievals (%) (DOFS>2 & RMS<5%) | 80 | 67 | 57 | 57 |

635



640 Figure 15. Example of NO₂ averaging kernels. They are calculated for observations on 11 September 2018 at 11:51 UTC and 300° azimuthal direction.



645

Figure 16. Example of the NO₂ measurement error in percentage for the 2 July 2018 at 05:59 UTC and 300° azimuthal direction.

5 Retrieval results and discussion

650 5.1 Example of daily horizontal NO₂ distribution

The variation of the MAX-DOAS horizontal distribution of tropospheric NO₂ VCDs as a function of time over the course of June 28 2019, is presented in Fig. 17. This particular day is chosen because airborne measurements took place above the Brussels region (see Sect. 5.2). The horizontal NO₂ profiles are plotted per azimuthal direction with the horizontal axis showing the time in UTC and the vertical axis the horizontal distance in km. Because of the quality check on the retrieved NO₂ horizontal profiles (see Sect. 4.3), some profiles were rejected (e.g. azimuthal direction equal to 262.5° and 265°).

655 During this day, maximum NO₂ columns are mainly observed around 05:00 UTC and 10:00 UTC, which correspond to 7am and noon local time. Early in the morning (05:00 UTC), high NO₂ columns are expected to be observed because of the low MLH (MLH_{NO₂} in the range of 300 – 600 m height) in combination with the morning rush hour NO₂ emissions. Around 10:00 UTC, the maximum NO₂ columns are detected in the north (N), northeast (NE), and northwest (NW) direction (see Fig. 18).
660 In the Brussels region, the main emission sources are located in the N and west (W) parts of the city and are linked to the motorway around Brussels (the so-called Ring), the Brussels city center, and the Drogenbos power plant (NW direction). Concerning the NO₂ peaks, they are located at a distance around 0 to 8 km from the measurement site. It can be seen from Fig. 18 that the Ring, the Brussels city center, and the Drogenbos power plant are located within these distances. As measured by



the meteorological station on the BIRA-IASB rooftop, the wind was coming from the NE direction during that day, resulting in the progressive displacement of the NO₂ peak from the NNE to the W direction. On the contrary, the azimuthal directions pointing towards a large forested area (i.e., 62.5°, 75°, and 105°), the Bois de la Cambre, detect considerably lower NO₂ columns than the other directions.

670

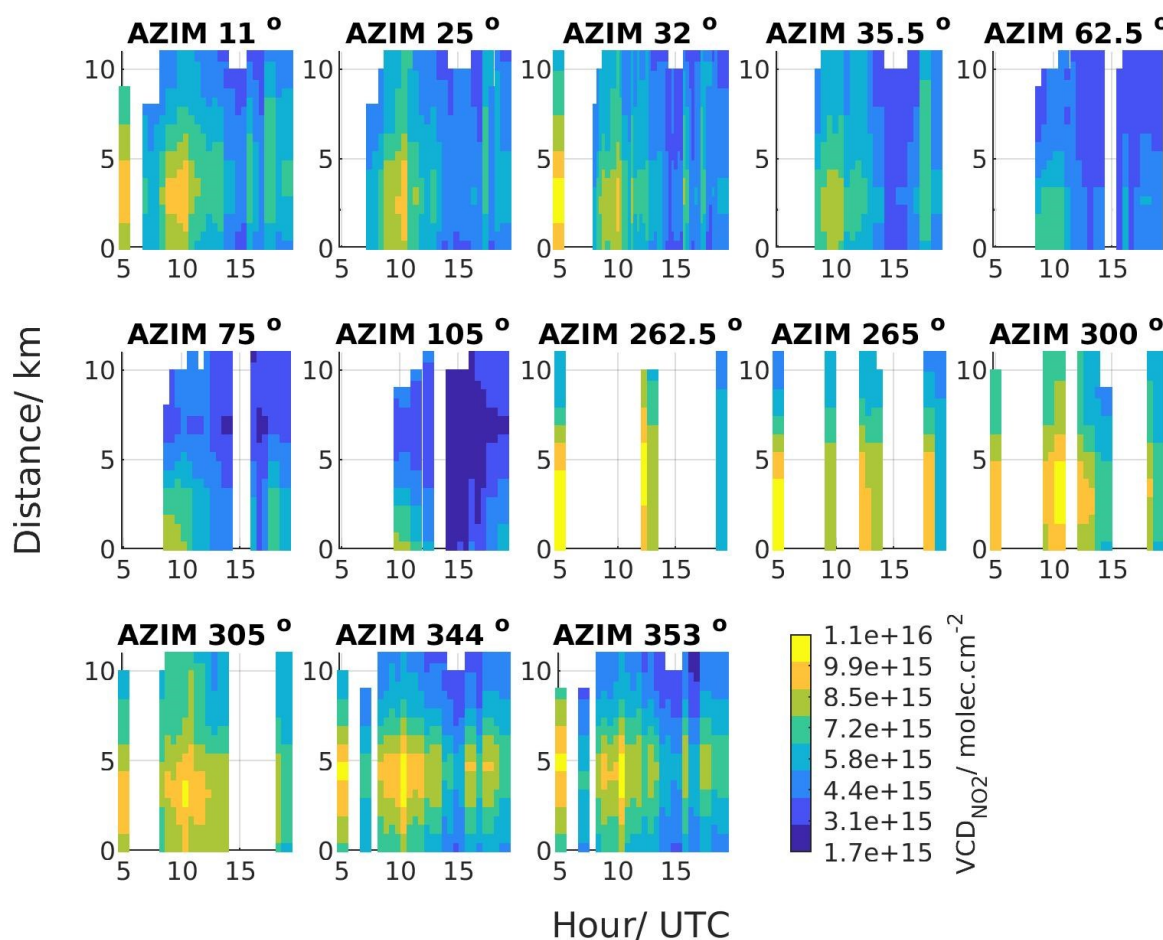
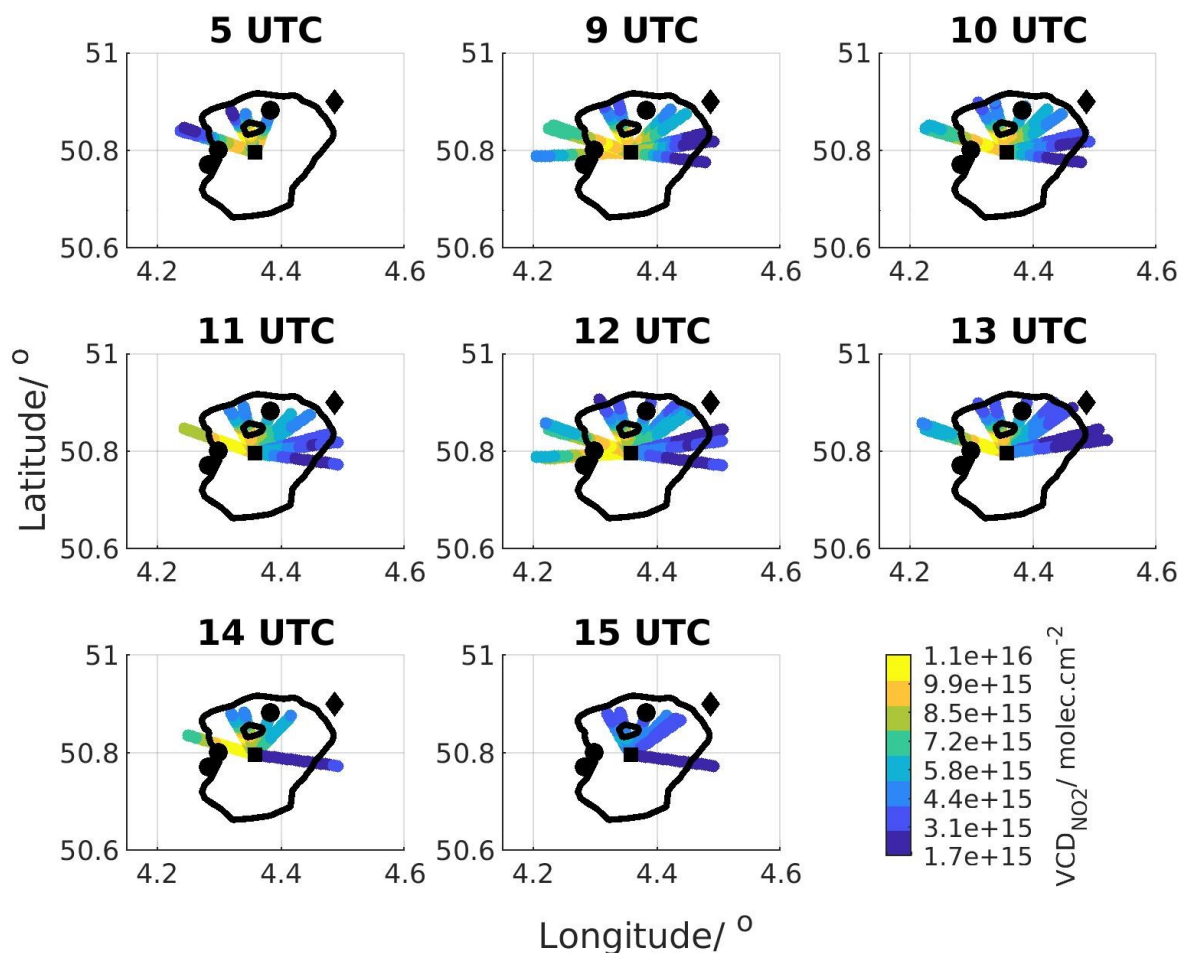


Figure 17. Diurnal variation of the retrieved NO₂ horizontal profiles per azimuthal direction as a function of time (UTC) for June 28, 2019.

675



680 **Figure 18.** Maps of hourly averaged NO_2 horizontal profiles per azimuthal direction for June 28, 2019 corresponding to Fig. 17. The wind direction was coming from the NE direction. The black square shows the MAX-DOAS instrument location, the black polygon the National Airport, the black dots the NO_2 hotspots emitting more than 10 kg of NO_x per hour (Emission Inventory of the Belgian Interregional Environment Agency, 2017), and the black line represents the Brussels Ring road.



685

5.2 MAX-DOAS horizontal NO₂ distribution versus airborne, car mobile-DOAS, and TROPOMI: 28 June 2019 case study

For the S5P validation campaign over Belgium (S5PVAL-BE, <https://s5pcampaigns.aeronomic.be/>), airborne measurements of the two largest urban regions over Belgium, i.e., Antwerp and Brussels, took place from 26 to 29 June 2019 (Tack et al., 2021). The Airborne Prism EXperiment (APEX) imaging spectrometer was used to measure the horizontal distribution of tropospheric NO₂ columns with a spatial resolution of approximately 75 m x 120 m (Tack et al., 2017; Tack et al., 2019).

The APEX tropospheric NO₂ columns are compared to the tropospheric NO₂ horizontal distribution as retrieved by applying our new MAX-DOAS inversion approach to the 28 June 2019 measurements. During the same day, TROPOMI pixels (OFFL 010302 product; see Table 1) selected over the Brussels region are compared to MAX-DOAS observations. MAX-DOAS horizontal profiles of tropospheric NO₂ VCDs are selected around TROPOMI overpass time (± 1 hour). The horizontal profile of MAX-DOAS NO₂ VCDs on each horizontal line-of-sight has a horizontal sampling of 0.5 km (see Fig. 13b). The MAX-DOAS NO₂ VCDs on the horizontal segment crossing a TROPOMI pixel and located inside the pixel are averaged and compared to the corresponding TROPOMI NO₂ VCD. It should be noted that the MAX-DOAS segments are not weighted by their relative length inside each pixel. APEX observations located inside each TROPOMI pixel were used to assign one APEX NO₂ VCD value per pixel. Maps of co-located TROPOMI, averaged MAX-DOAS, and averaged APEX NO₂ VCDs for the 28 June 2019 are shown in Fig. 19. Two maps of APEX observations are presented: one with APEX in its initial resolution and one with spatially averaged APEX observations in the area covered by a TROPOMI pixel. The NO₂ plume as detected by APEX is covering the NW, N, and NE parts of the Brussels region. MAX-DOAS successfully detected the same NO₂ plume in the NW and N but not in the NE direction. The correlation and agreement between APEX and MAX-DOAS observations is very good ($R=0.83$ and $s=1.10$). As we can observe in Fig. 20, the APEX tropospheric NO₂ VCDs tend to be larger than the MAX-DOAS ones, with an intercept equal to -2.10×10^{15} molec.cm².

During the S5PVAL-BE flight over Brussels, car mobile-DOAS observations were performed by the BIRA-IASB mobile-DOAS, the so-called AEROMOBIL (Merlaud, 2013). The AEROMOBIL consists of a compact double Avantes spectrometer recording simultaneously scattered light in two channels (i.e., one at 30° elevation angle and one at zenith). The AEROMOBIL was used to measure the spatial distribution of tropospheric NO₂ columns mainly over the Ring road of Brussels. Similarly as with APEX, the AEROMOBIL NO₂ VCDs, which are located inside a TROPOMI pixel are averaged and compared to the corresponding MAX-DOAS VCDs (see Fig. 19e and 19f). AEROMOBIL and MAX-DOAS agree perfectly on the location of maximum (i.e. NW direction) and minimum (i.e. SE direction) NO₂ tropospheric VCDs (Fig. 19d, 19e, and 19f). We can observe in Fig. 20b, that the correlation coefficient is moderate (R equal to 0.61) and the slope value is equal to 2.62. The correlation plot between both datasets reveals that AEROMOBIL gives higher NO₂ tropospheric VCDs compared to MAX-DOAS ones. This finding could be partly explained by the fact that AEROMOBIL follows busy routes, where the NO₂



tropospheric VCDs reach maximum values because of the contribution of NO₂ production resulted by vehicles' engines via fossil fuel combustion.

720 The correlation between TROPOMI and MAX-DOAS tropospheric NO₂ columns during the day of the airborne measurements above Brussels is presented in Fig. 20c. Excellent agreement is obtained, with a correlation coefficient value equal to 0.81. The slope value is equal to 0.72. During that day, MAX-DOAS and TROPOMI are in good agreement but TROPOMI tends to underestimate the tropospheric NO₂ columns. It should be noted that during that day, the range of observed NO₂ VCDs is from 3.4×10^{15} to 8.7×10^{15} molec.cm⁻², as retrieved by the MAX-DOAS observations.

725

730

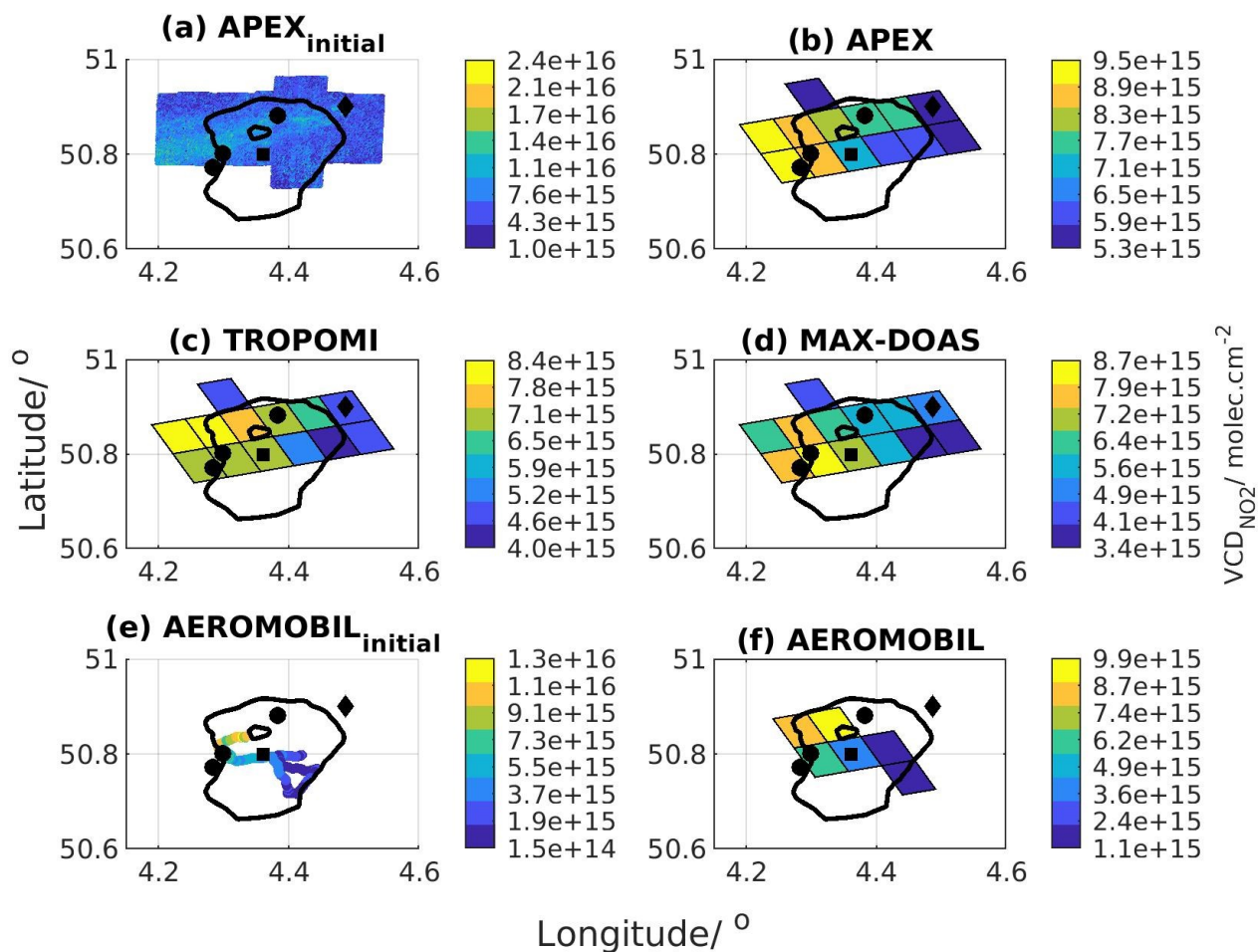
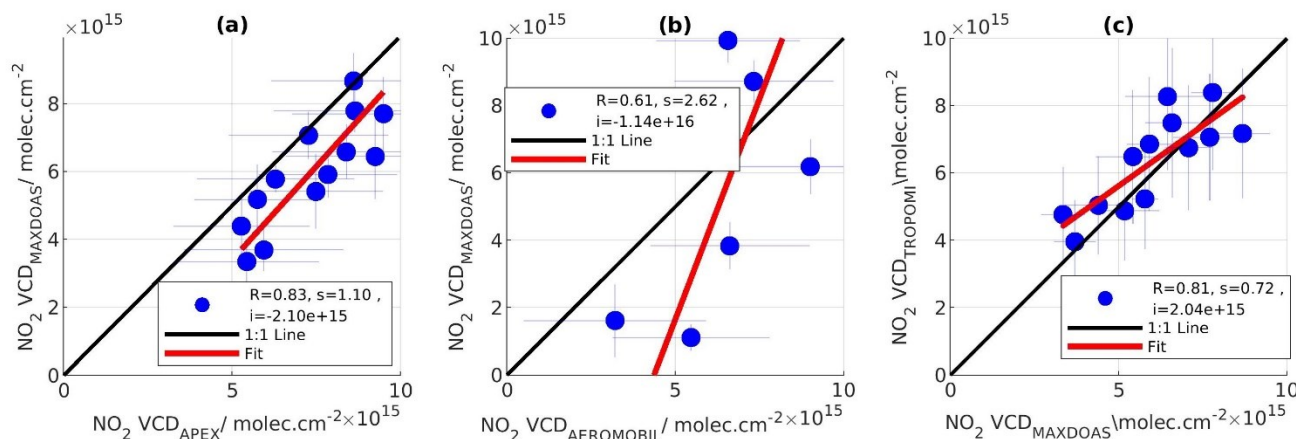


Figure 19. (a) Tropospheric NO₂ VCD as detected by the APEX instrument in its initial spatial resolution. Tropospheric NO₂ VCD maps (TROPOMI pixels) as retrieved over Brussels on 28th of June 2019 by the (b) APEX, (c) TROPOMI, (d) MAX-DOAS instruments. (e) Tropospheric NO₂ VCD as retrieved by the AEROMOBIL in its initial spatial resolution and (f) AEROMOBIL tropospheric NO₂ VCD in the TROPOMI pixels. The black square shows the MAX-DOAS instrument location, the black polygon the National Airport, the black dots the NO₂ hotspots emitting more than 10 kg of NO_x per hour (Emission Inventory of the Belgian Interregional Environment Agency, 2017), and the black line represents the Brussels Ring road.

735
740



745 **Figure 20.** Scatter plot between (a) the tropospheric NO₂ columns derived by airborne measurements (APEX) and the
 MAX-DOAS observations, (b) the tropospheric NO₂ columns derived by car mobile-DOAS measurements
 (AEROMOBIL), and the MAX-DOAS observations and (c) the tropospheric NO₂ columns derived by MAX-DOAS
 observations and the TROPOMI tropospheric NO₂ columns over Brussels on 28th of June 2019.

750

5.3 MAX-DOAS horizontal NO₂ distribution versus TROPOMI observations

5.3.1 Comparison results of the March 2018-February 2020 period

To compare the TROPOMI and MAX-DOAS tropospheric NO₂ columns, the following 5-step approach is used, similarly as in Section 5.2:

- 755
1. Only MAX-DOAS horizontal profiles of tropospheric NO₂ VCDs retrieved around (± 1 hour) TROPOMI overpass time are selected.
 2. The time-coincident MAX-DOAS tropospheric NO₂ VCD horizontal grids from all the azimuthal directions are spatially averaged (i.e. one MAX-DOAS mean NO₂ VCD value per pixel) within the overlapping TROPOMI pixels.
 3. To take into account the distance between each azimuthal direction crossing a TROPOMI pixel and the TROPOMI pixel center, the MAX-DOAS average is a weighted mean with the weighting depending on their relative direction with respect to the direction of the TROPOMI pixel center. Consequently, the weights are equal to the difference between 360° and the azimuthal difference between MAX-DOAS grid and TROPOMI pixel central coordinates.
 4. The horizontal profiles of MAX-DOAS NO₂ columns have a horizontal sampling of 0.5 km in every azimuthal direction. The coverage percentage is estimated as the ratio of the area covered by MAX-DOAS (i.e., number of coincident MAX-DOAS NO₂ VCDs considering that every MAX-DOAS horizontal grid has a spatial resolution of 0.5 x 0.5 km²) inside each TROPOMI pixel to the total number of MAX-DOAS NO₂ VCDs that could fill-in the TROPOMI pixel.
- 760
- 765



5. TROPOMI and MAX-DOAS tropospheric NO₂ columns are compared, and the seasonally-averaged maps of those VCDs on the area covered by the TROPOMI pixels are created. To generate these maps, the ensemble of TROPOMI pixels recorded on 28 June 2019 is chosen as reference and TROPOMI pixels that coincide with this reference grid are averaged. The daily horizontal profiles of MAX-DOAS NO₂ columns are averaged on the daily TROPOMI grids and then, the reference grid is used to create the seasonally-averaged MAX-DOAS maps.

The seasonally and annually-averaged maps of TROPOMI and MAX-DOAS NO₂ VCDs are presented in Fig. 21 and Fig. 22. Only pixels including at least 20 comparison days are taken into account in the analysis. It is found that the locations of the NO₂ peaks and dips show a reasonably high degree of similarity between TROPOMI and MAX-DOAS during all seasons. The NO₂ peaks appear mainly above Brussels city center, the Drogenbos power plant (W direction) and the NW part of the Ring road, which are the main known emission sources, as mentioned earlier. These maps also indicate that the tropospheric NO₂ column over the Brussels area has a clear seasonal cycle, with a maximum during winter.

Figure 22c shows the annual relative biases (e.g., $100 \times (\text{TROPOMI} - \text{MAX-DOAS})/\text{MAX-DOAS}$) per pixel. It is found that positive biases (i.e. TROPOMI larger than MAX-DOAS) are observed mainly in the pixels located away from the measurement site during all seasons, while negative biases are found close to the measurement site and in the Brussels city center.

The seasonal correlation plots for April 2018-February 2020 are displayed in Fig. 23. When all pixels are included, without any TROPOMI pixels coverage percentage filtering on MAX-DOAS data, the highest correlation is found during spring ($R=0.66$), while lower correlations are reported in autumn, summer, and winter, with correlation coefficient values of 0.65, 0.65, and 0.58, respectively. It should be noted that during spring (2018 and 2019), the number of comparison points is smaller than for the other seasons, because TROPOMI data start from end of April 2018. During spring, the slope value is equal to 0.90, while during winter, summer, and autumn, the slope values are smaller (0.64 0.56, and 0.64, respectively), which means that TROPOMI underestimates MAX-DOAS measurements up to 50 %. A similar underestimation has been reported in several studies (Verhoelst et al., 2021; Tack et al., 2021; Judd et al., 2020; Dimitropoulou et al., 2020; Ialongo et al., 2019). When seasonally-averaged TROPOMI and MAX-DOAS pixels (the pixels shown in Fig. 21) are compared one-by-one (see SEAS in Fig. 23), both correlation coefficient (R in the range of 0.57-0.93) and slope values (s in the range of 0.65-0.94) improve considerably.

In a second step, the impact of the spatial sampling is investigated. Generally, a varying number of MAX-DOAS NO₂ columns cover each TROPOMI pixel. The coverage percentage is estimated as the ratio of the covered area by MAX-DOAS (i.e., number of coincident MAX-DOAS NO₂ VCDs) inside each TROPOMI pixel to the total number of MAX-DOAS NO₂ VCDs that could fill-in the TROPOMI pixel. When selecting only TROPOMI pixels covered by at least a given percentage of MAX-DOAS grids (10% and 20%), it is found that the correlation between both datasets improves for all seasons, except summer for a coverage equal and greater than 20%. The most significant improvement is observed during spring. The correlation coefficient value is equal to 0.83 (instead of 0.66) when taking into account TROPOMI pixels covered more than 20% by

MAX-DOAS retrievals. Despite the better agreement in terms of correlation coefficient, TROPOMI columns are still 30 % lower than MAX-DOAS measurements, in line with previously published studies.

805 The seasonal regression analysis parameters between TROPOMI and dual-scan MAX-DOAS measurements derived in the present study are compared to the same parameters presented in Dimitropoulou et al. (2020). Both studies make use of the dual-scan MAX-DOAS instrument in Uccle. In addition to the different approach (i.e., the retrieval of NO₂ horizontal profiles), in the present study, almost two years of measurements are used, while in Dimitropoulou et al. (2020), only one year is exploited for the TROPOMI validation. In Table 4, for the present study, only one year of measurements are used to have a
810 comparable time coverage for both studies. As presented in Table 4, here, the largest slope value is found in spring, while in Dimitropoulou et al. (2020), in winter. The season in which the highest correlation coefficient is obtained differs between both studies (here, in spring, in autumn in Dimitropoulou et al. (2020)). The main advantage of the new approach is the larger number of comparison points between TROPOMI and MAX-DOAS leading to significantly more reliable statistics. In the present study, the deviation of the comparison points from the fitted regression line is increased mainly because of the
815 uncertainties in the horizontal inversion approach. The scatter increase is reflected in the correlation coefficient values, which are smaller for all seasons, except winter. Regarding the slope value, it is larger in spring and summer, and is smaller in autumn and winter.

Overall, our investigation about the spatial sampling lead to the following three important findings:

- 820
1. The dual-scan multi-wavelength approach allows a better identification of the main emissions sources in urban regions, in agreement with the spatial allocation of the main emission sources observed by APEX and TROPOMI.
 2. The characterization of the NO₂ concentration horizontal field using the dual scan multi-wavelength approach results in obtaining larger slope values between TROPOMI and MAX-DOAS observations. The high spatial resolution of TROPOMI requires ground-based measurement that can provide information about the horizontal distribution of
825 tropospheric NO₂ columns in urban regions.
 3. Even for a better spatial sampling between TROPOMI and ground-based observations, TROPOMI still underestimates the ground-based measurements (see Fig. 22). Therefore, this is an additional indication that this underestimation is caused by other factors.

830

835

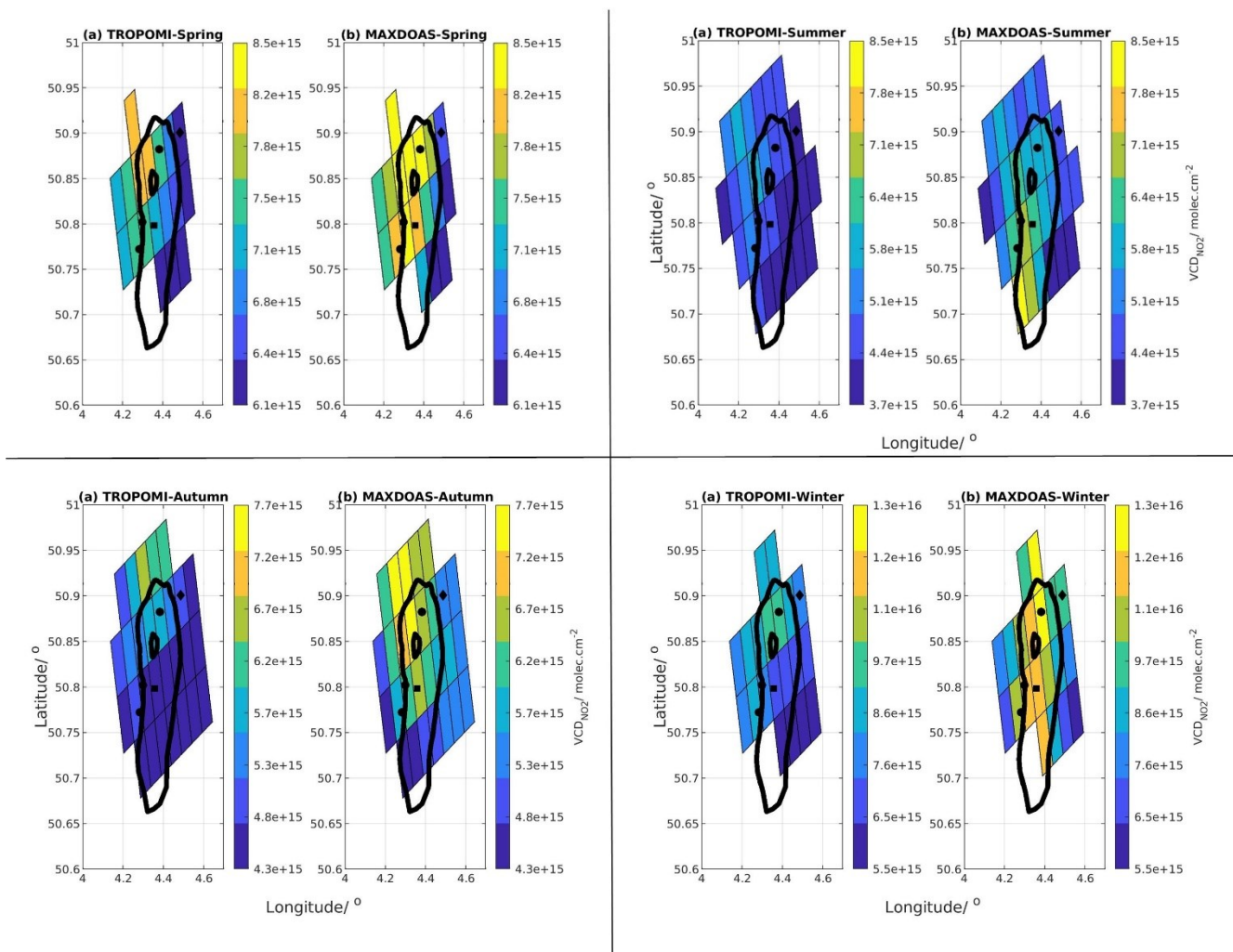


Figure 21. Seasonal tropospheric NO₂ VCD grids (TROPOMI grids) as retrieved over Brussels by the TROPOMI and MAX-DOAS instruments. The black square shows the MAX-DOAS position, the black polygon the National Airport, the black dots the NO₂ hotspots, and the black line represents the Brussels Ring motorway.

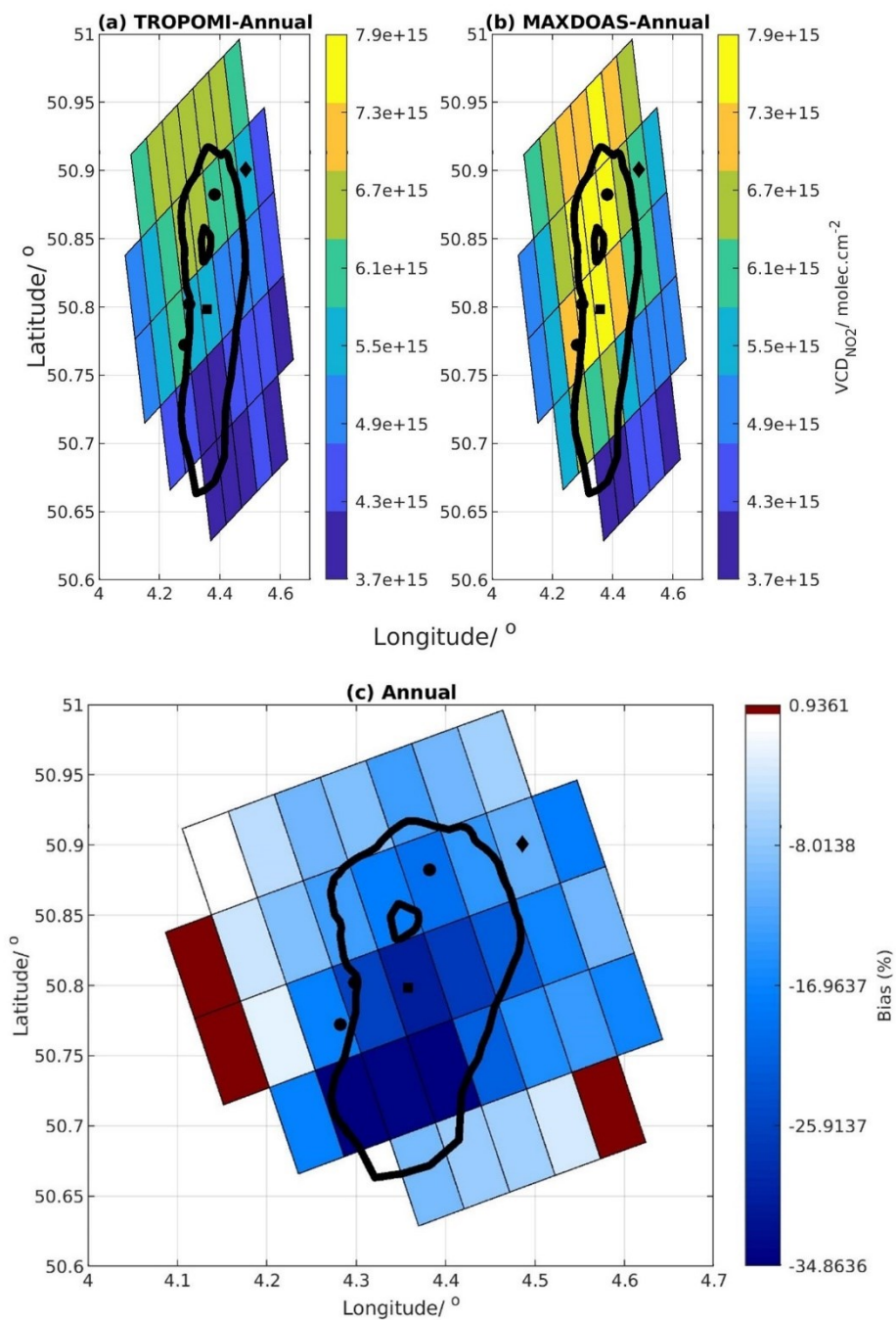


Figure 22. Annual (e.g., based over the two years of observations) tropospheric NO₂ VCD grids (TROPOMI grids) as retrieved over Brussels by the (a) TROPOMI and (b) MAX-DOAS instruments. (c) Annual bias between tropospheric

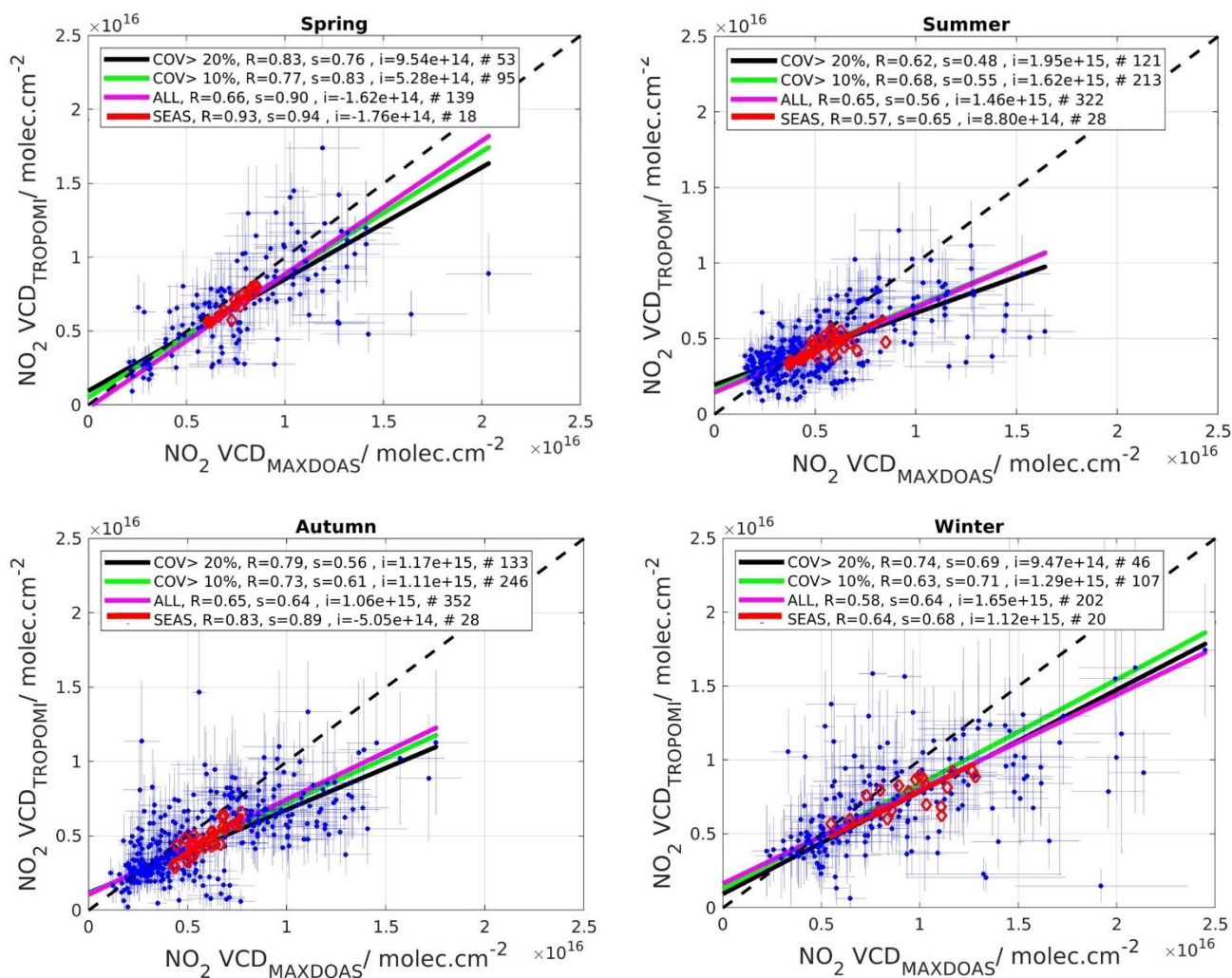


845 **NO₂ VCD as observed by TROPOMI and MAX-DOAS instruments (the negative values are shown with blue color, zero with white, and positive values with red). The black square shows the MAX-DOAS instrument location, the black polygon the National Airport, the black dots the NO₂ hotspots, and the black line represents the Brussels Ring road.**

850

855

860



865 **Figure 23.** Seasonal scatter plots of tropospheric NO₂ columns derived from the dual-scan MAX-DOAS and TROPOMI measurements over Brussels. Magenta line: Regression analysis results when all the MAX-DOAS and TROPOMI pixels are included in the comparison. Green and black lines: Regression analysis results when TROPOMI pixels covered (i.e., COV) by more than 10 and 20 % of the horizontal profiles of MAX-DOAS NO₂ columns are included in the comparison. Red line: Seasonal average analysis generated by the pixels in Fig. 21.

870



875

Table 4. Summary of the regression analysis parameters (e.g., correlation coefficient (R) and slope (s)) and the number of data points (N) derived in the present study during only one year of observations and in Dimitropoulou et al. (2020).

880

| Season | Spring | Summer | Autumn | Winter |
|---------------------------------------|--------|--------|--------|--------|
| R | 0.66 | 0.60 | 0.57 | 0.62 |
| R (seasonal) | 0.93 | 0.88 | 0.46 | 0.75 |
| R (Dimitropoulou et al., 2020) | 0.69 | 0.77 | 0.85 | 0.60 |
| s | 0.90 | 0.76 | 0.56 | 0.60 |
| s (seasonal) | 0.94 | 0.87 | 0.74 | 0.70 |
| s (Dimitropoulou et al., 2020) | 0.47 | 0.58 | 0.61 | 0.81 |
| N | 139 | 247 | 106 | 92 |
| N (Dimitropoulou et al., 2020) | 16 | 58 | 36 | 13 |

5.3.2 Investigation of the a priori NO₂ profile shape and clouds in TROPOMI NO₂ retrievals

Three additional comparisons were conducted in this study. First, a TROPOMI tropospheric NO₂ column product with an improved FRESKO-S cloud retrieval was tested. As discussed in Dimitropoulou et al. (2020), clouds can significantly affect tropospheric NO₂ VCD retrievals from satellite observations. The dataset is available for four different periods in 2018 – 2019 (see Sect. 3). Fig. 24 shows that the slope value increases by about 56% (equal to 0.53 instead of 0.34 for the baseline product), as well as the correlation coefficient between both datasets (R equal to 0.68 instead of 0.45). This is in agreement with the TROPOMI Routine Operations Consolidated Validation Report (ROCVR; <https://mpc-vdaf.tropomi.eu/>), where the use of the improved FRESKO-wide resulted in a bias reduction with respect to ground-based NO₂ data.

890

Secondly, a new TROPOMI data product covering the November 2018 to February 2020 period is used. In this product, the coarse TM5-MP a priori NO₂ profiles are replaced by NO₂ profile shapes from the CAMS regional CTM ensemble at a spatial resolution of 0.1° x 0.1° (Douros et al., in preparation; Ialongo et al., 2019; Tack et al., 2021). As can be seen in Fig. 24, using a spatially finer a priori NO₂ vertical profile improves slightly the slope value, which is equal to 0.77 (instead of 0.75 for the baseline TROPOMI product). This represents an increase of the slope by about 3%. This finding indicates that part of the TROPOMI underestimation of tropospheric NO₂ columns is caused by inadequate a priori profiles in the TROPOMI retrievals

895



for urban conditions. On the other hand, the fact that the slope value is still lower than unity, even when CAMS regional a priori profiles are used, indicate that other factors contribute to the TROPOMI underestimation or that CAMS profiles are still sub-optimal, as suggested by results obtained when applying MAX-DOAS profiles to TROPOMI (see below).

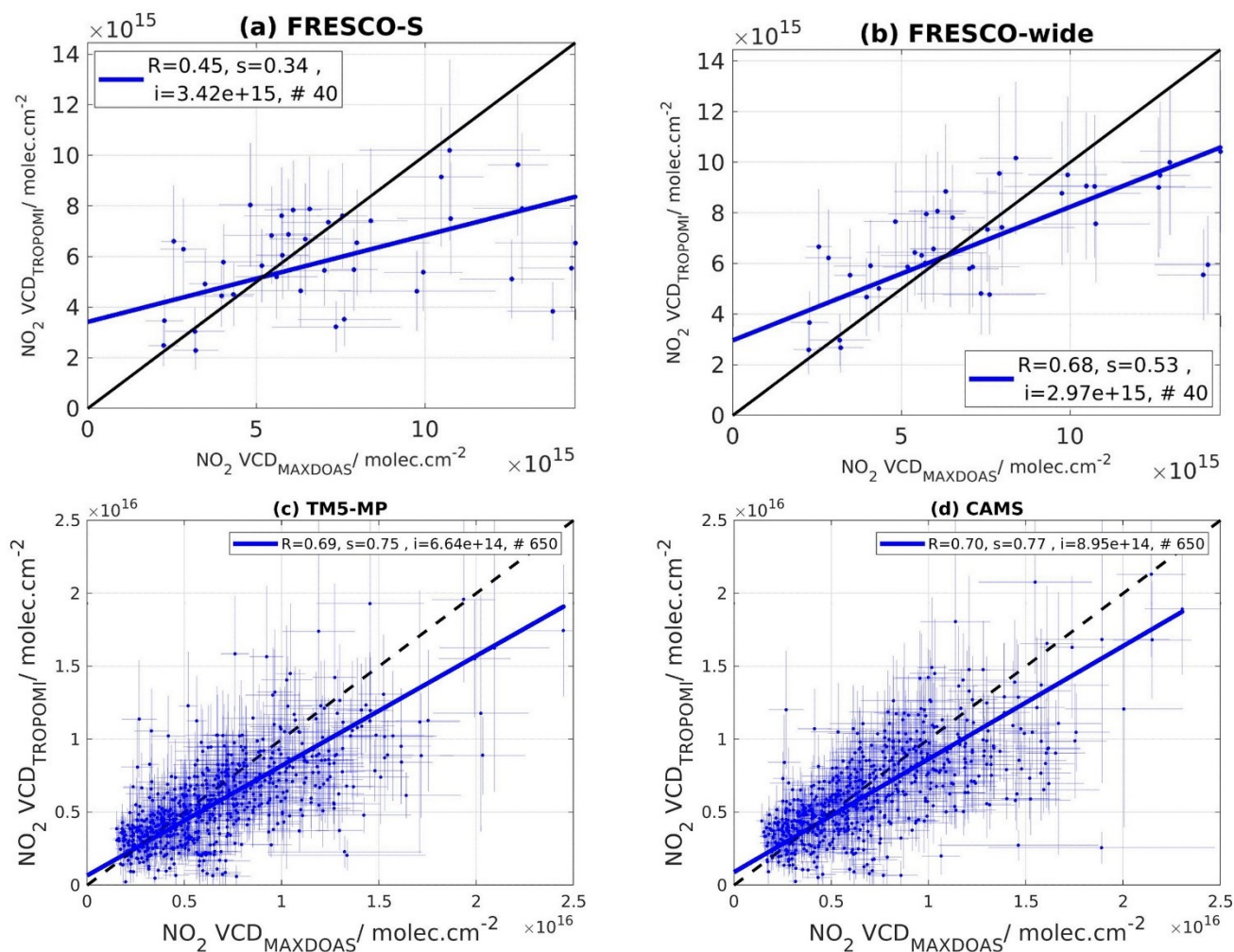
900 Finally, the impact of the a priori profile in the TROPOMI NO₂ retrieval is investigated using MAX-DOAS profile data. For this test, TROPOMI NO₂ columns are recalculated, similarly as in Dimitropoulou et al. (2020), using daily median MAX-DOAS vertical profiles derived in the main azimuthal direction by applying the MMF inversion algorithm. Those TROPOMI NO₂ columns are then compared to the horizontally-resolved MAX-DOAS data, as in Sect. 5.3.1. Figure 25 presents the comparison results per season. When comparing it with Fig. 23, we find that the change in the NO₂ vertical profile shape

905 improves the slope value in the comparison with ground-based observations. Except for winter, the slopes are largely improved (slopes in the 0.56 - 1.11 range) due to an increase of the recalculated TROPOMI columns. This result confirms once again that the a priori profile in the TROPOMI retrieval is a key player in the TROPOMI underestimation of tropospheric NO₂ columns in urban conditions, as already stated in previous studies (see e.g. Dimitropoulou et al., 2020; Ialongo et al., 2019; Tack et al., 2021). The present study suggests that in urban conditions, daily median MAX-DOAS vertical profiles are more

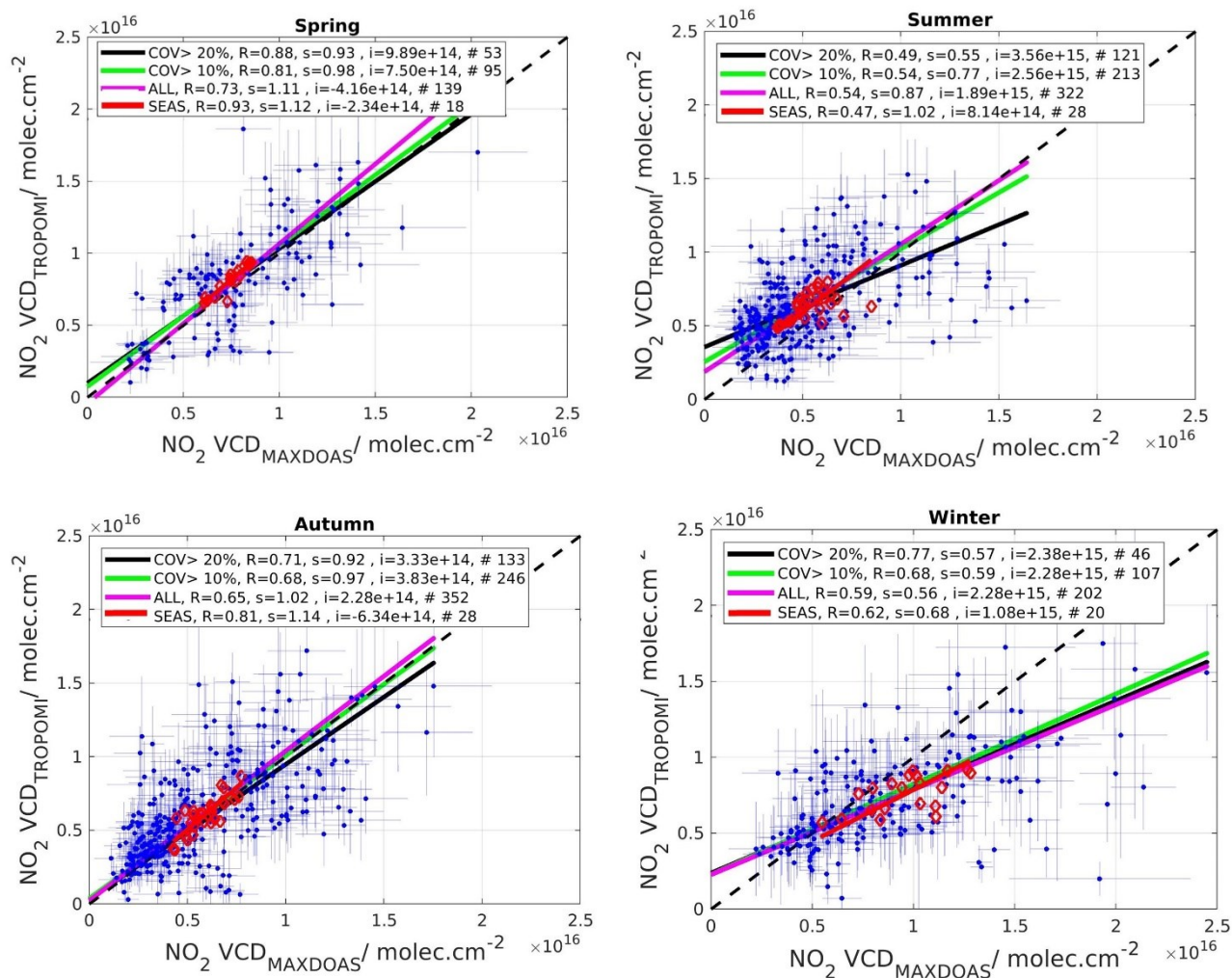
910 suitable than NO₂ profile shapes from the CAMS regional CTM ensemble in order to be applied as a priori information in the TROPOMI retrieval.

915

920



925 **Figure 24.** Scatter plots between the tropospheric NO_2 columns derived from the dual-scan MAX-DOAS instrument
and the TROPOMI pixels over Brussels. The left plots are for the baseline TROPOMI dataset ((a) and (c) panels), while
the right plots correspond to two new versions of TROPOMI datasets ((b): improved FRESCO-S cloud product; (d)
930 NO_2 a priori profiles from the CAMS regional CTM ensemble).
935



940 **Figure 25.** Seasonal scatter plots between the horizontally-averaged MAX-DOAS NO₂ VCDs and TROPOMI NO₂ columns recalculated using median daily MAX-DOAS vertical profiles as a priori information.

6 Conclusions

Two years (March 2018 to February 2020) of dual-scan MAX-DOAS measurements in Uccle (urban background site located in the south of the Brussels-Capital Region) were used to develop a new strategy for the retrieval of near-surface NO₂ concentrations and aerosol extinction horizontal profiles. A full dual-scan measurement is composed of one vertical scan at a fixed azimuthal direction pointing towards the city center and horizontal scans in ten azimuthal directions at a fixed low elevation angle (2°).



The first step of this new retrieval strategy is to analyze measured radiance spectra in six different fitting windows. This provides O_4 and NO_2 dSCDs at the following six wavelengths: 343 nm, 360 nm, 380 nm, 447 nm, 477 nm and 530 nm. Then, information about the vertical extent of NO_2 in the troposphere (MLH_{NO_2}) is derived from profile retrievals in the main azimuthal direction performed using the OEM-based MMF algorithm. In the third step, a new parameterization technique is applied, with MLH_{NO_2} , measured O_4 dSCDs, and measurement geometry being used as input parameters to retrieve the horizontal sensitivity of NO_2 and, consequently, the NO_2 near-surface concentrations and VCDs, and near-surface aerosol extinction in all the azimuthal directions for the six different wavelengths. Compared to the method presented in Dimitropoulou et al., (2020), the new retrieval method offers the possibility of the direct determination of L_{NO_2} , and near-surface aerosol extinction based on the measured O_4 dSCDs.

The retrieved dual-scan NO_2 near-surface concentrations and VCDs are verified via comparisons to the MMF NO_2 vertical profiles in the main azimuthal directions and in three additional azimuthal directions. A good overall agreement is found for the two comparisons during the two years of measurements.

The dependence of the horizontal sensitivity on the wavelength is then used to develop a new OEM-based horizontal distribution inversion approach. Considering a horizontal box model, horizontal NO_2 and aerosol extinction profiles are retrieved in an output horizontal grid of 500m thickness starting from the instrument to each of the measurement maximum horizontal representative distance.

The daily variability of NO_2 horizontal profiles in all the azimuthal directions provides information about the location of the NO_2 hotspots in the Brussels-Capital Region and how the plumes are transported. Similarly, the NO_2 horizontal profiles' seasonal variability over March 2018-February 2020 reveals that the NO_2 hotspots are mainly found above the Brussels city-center, the Drogenbos power plant and the NW part of the Ring road during all seasons.

On 28 June 2019, airborne measurements (APEX) of NO_2 were performed over Brussels. The MAX-DOAS NO_2 VCD horizontal profiles are compared to APEX, mobile car-DOAS (i.e., AEROMOBIL), and TROPOMI measurements, and a good overall agreement is found between the different data sets for this day.

In the second part of the study, MAX-DOAS retrievals are compared to TROPOMI tropospheric NO_2 observations over the March 2018- February 2020 period. The comparison of seasonal maps shows a good overall agreement between both datasets as to the NO_2 horizontal distribution over the Brussels area. This agreement improves systematically when only TROPOMI pixels covered by a minimum of 20% of MAX-DOAS grid cells are compared, showing the benefit of ground-based measurements at high horizontal resolution for the validation of high-resolution space-borne air-quality measurements. Results also show that during all seasons, TROPOMI underestimates the MAX-DOAS tropospheric NO_2 columns. The role of the a priori NO_2 profile shape in the TROPOMI retrievals was investigated and TROPOMI tropospheric NO_2 columns are recalculated with the MAX-DOAS vertical profiles. We show that the knowledge of the NO_2 horizontal distribution derived by the MAX-DOAS measurements combined with a more adequate a priori profile in TROPOMI retrievals leads to a much better agreement between satellite and ground-based data.



To conclude, our study presents a new horizontal distribution inversion approach for NO₂ and aerosols developed by using dual-scan multi-wavelength MAX-DOAS measurements over an urban area. This approach provides a better characterization of the horizontal distribution of an important urban pollutant, NO₂, which leads to an improved agreement between satellite and MAX-DOAS measurements in moderate to highly polluted conditions. Based on our study, further modifications of the measurement mode aiming at a better sampling of the vertical and horizontal NO₂ distribution could be implemented and investigated. For instance, performing vertical scans in several azimuthal directions throughout the day and/or horizontal scans in more than ten azimuthal directions could further improve our knowledge about the tropospheric NO₂ spatial variability in urban regions, and therefore the satellite validation results in those conditions.

Data availability. The datasets generated and analyzed in the present work are available from the corresponding author on request.

Author contributions. ED undertook the development and validation of the dual-scan multi-wavelength MAX-DOAS retrieval strategy in Uccle, exploited the MAX-DOAS retrievals during two year, performed the validation of the TROPOMI tropospheric NO₂ columns, and wrote the paper. FH supported and guided ED in the development of the dual-scan multi-wavelength MAX-DOAS retrieval strategy, provided general guidelines, and revised and edited the paper. MMF provided the MMF inversion algorithm and the RTM as well as supporting and guiding ED in the new OEM-based horizontal profile retrieval. FT provided the airborne APEX dataset and contributed to scientific discussions. GP provided the dataset of the TROPOMI tropospheric NO₂ columns and supported ED in the TROPOMI validation approaches. AM provided the AEROMOBIL dataset and contributed to scientific discussions. CF and CH provided technical and software support for the MAX-DOAS instrument in Uccle. CF developed the QDOAS software and guided ED in the DOAS analysis. FF provided the RIO model dataset. MVR supervised the present work, provided general guidelines and valuable comments during the whole process of the paper preparation, and revised and edited the paper. All authors reviewed, discussed and commented on the paper.

1005

Competing interests. I declare that I or my co-authors have competing interests as follows: Michel Van Roozendael is associate editor of AMT.

1010

References

Aliwell, S.R., Van Roozendael, M., Johnston, P.V., Richter, A., Wagner, T., Arlander, D.W., Burrows, J.P., Fish, D.J., Jones,



- 1015 R.L., Tørnkvist, K.K. and Lambert, J.C., 2002. Analysis for BrO in zenith-sky spectra: An intercomparison exercise for analysis improvement. *Journal of Geophysical Research: Atmospheres*, 107(D14), pp.ACH-10.
- Barret, B., De Maziere, M., and Demoulin, P.: Retrieval and characterisation of ozone profiles from solar infrared spectra at the Jungfraujoch, *J. Geophys. Res.*, 107 (D24), 4788, doi:10.1029/2001JD001298, 2002.
- Beirle, S., Dörner, S., Donner, S., Remmers, J., Wang, Y., and Wagner, T.: The Mainz profile algorithm (MAPA), *Atmos. Meas. Tech.*, 12, 1785–1806, <https://doi.org/10.5194/amt-12-1785-2019>, 2019.
- 1020 Beirle, S., Platt, U., Wenig, M., and Wagner, T.: Weekly cycle of NO₂ by GOME measurements: a signature of anthropogenic sources, *Atmos. Chem. Phys.*, 3, 2225–2232, <https://doi.org/10.5194/acp-3-2225-2003>, 2003.
- Bösch, T., Rozanov, V., Richter, A., Peters, E., Rozanov, A., Wittrock, F., Merlaud, A., Lampel, J., Schmitt, S., de Haij, M., Berkhout, S., Henzing, B., Apituley, A., den Hoed, M., Vonk, J., Tiefengraber, M., Müller, M., and Burrows, J. P.: BOREAS – a new MAX-DOAS profile retrieval algorithm for aerosols and trace gases, *Atmos. Meas. Tech.*, 11, 6833–6859, <https://doi.org/10.5194/amt-11-6833-2018>, 2018.
- 1025 Burrows, J. P., Weber, M., Buchwitz, M., Rosanov, V. V., Ladstätter, A., Weissenmayer, A., Richter, A., DeBeek, R., Hoogen, R., Bramstedt, K., and Eichmann, K. U.: The Global Ozone Monitoring Experiment (GOME): Mission concept and first scientific results, *J. Atmos. Sci.*, 56, 151–175, 1999.
- Chance, K. V. and Spurr, R. J. D.: Ring effect studies: Rayleigh scattering, including molecular parameters for rotational Raman scattering, and the Fraunhofer spectrum, *Appl. Optics*, 36, 5224–5230, doi:10.1364/AO.36.005224, 1997.
- 1030 Chan, K. L., Wiegner, M., van Geffen, J., De Smedt, I., Alberti, C., Cheng, Z., Ye, S., and Wenig, M.: MAX-DOAS measurements of tropospheric NO₂ and HCHO in Munich and the comparison to OMI and TROPOMI satellite observations, *Atmos. Meas. Tech.*, 13, 4499–4520, <https://doi.org/10.5194/amt-13-4499-2020>, 2020.
- Chen, T. M., Kuschner, W. G., Gokhale, J., & Shofer, S. (2007). Outdoor air pollution: nitrogen dioxide, sulfur dioxide, and carbon monoxide health effects. *The American journal of the medical sciences*, 333(4), 249-256.
- 1035 Clémer, K., Van Roozendaal, M., Fayt, C., Hendrick, F., Hermans, C., Pinardi, G., Spurr, R., Wang, P., and De Mazière, M.: Multiple wavelength retrieval of tropospheric aerosol optical properties from MAXDOAS measurements in Beijing, *Atmos. Meas. Tech.*, 3, 863–878, <https://doi.org/10.5194/amt-3-863-2010>, 2010.
- Compernelle, S., Argyrouli, A., Lutz, R., Sneep, M., Lambert, J.-C., Fjæraa, A. M., Hubert, D., Keppens, A., Loyola, D., O'Connor, E., Romahn, F., Stammes, P., Verhoelst, T., and Wang, P.: Validation of the Sentinel-5 Precursor TROPOMI cloud data with Cloudnet, Aura OMI O₂–O₂, MODIS, and Suomi-NPP VIIRS, *Atmos. Meas. Tech.*, 14, 2451–2476, <https://doi.org/10.5194/amt-14-2451-2021>, 2021.
- 1040 Dimitropoulou, E., Hendrick, F., Pinardi, G., Friedrich, M. M., Merlaud, A., Tack, F., De Longueville, H., Fayt, C., Hermans, C., Laffineur, Q., Fierens, F., and Van Roozendaal, M.: Validation of TROPOMI tropospheric NO₂ columns using dual scan multi-axis differential optical absorption spectroscopy (MAX-DOAS) measurements in Uccle, Brussels, *Atmos. Meas. Tech.*, 13, 5165–5191, <https://doi.org/10.5194/amt-13-5165-2020>, 2020.
- 1045 Douros, J., Eskes, H., van Geffen, J., Boersma, F., Compernelle, S., Pinardi, G., Blechschmidt, A.-M., Peuch, V.-H., Colette,



- A., and Veeffkind P.: Comparing Sentinel-5P TROPOMI NO₂ column observations with the CAMS-regional air quality ensemble, in preparation.
- 1050 Eskes, H. J., van Geffen, J., Boersma, K. F., Sneep, M., ter Linden, M., Richter, A., Beirle, S. and Veeffkind, J. P.: High spatial resolution nitrogen dioxide tropospheric column observations derived from Sentinel-5P TROPOMI observations, *Atmos. Meas. Tech.*, in preparation, 2020.
- Eskes, H. J. and K. U. Eichmann (2020), S5P Mission Performance Centre Nitrogen Dioxide [L2__NO2__] Readme, Rep. 02.02.00, S5P-MPC-KNMI-PRF-NO2, 5 July 2021, <https://sentinel.esa.int/documents/247904/3541451/Sentinel-5P-Nitrogen-Dioxide-Level-2-Product-Readme-File>.
- 1055 Fayt, C., De Smedt, I., Letocart, V., Merlaud, A., Pinardi, G., and Van Roozendael, M.: QDOAS Software user manual, <http://uv-vis.aeronomie.be/software/QDOAS/index.php>, 2011.
- Fleischmann, O. C., Hartmann, M., Burrows, J. P., and Orphal, J.: New ultraviolet absorption cross-sections of BrO at atmospheric temperatures measured by time-windowing Fourier transform spectroscopy, *J. Photoch. Photobio. A*, 168, 117–132, 2004.
- 1060 Friedrich, M. M., Rivera, C., Stremme, W., Ojeda, Z., Arellano, J., Bezanilla, A., García-Reynoso, J. A., and Grutter, M.: NO₂ vertical profiles and column densities from MAX-DOAS measurements in Mexico City, *Atmos. Meas. Tech.*, 12, 2545–2565, <https://doi.org/10.5194/amt-12-2545-2019>, 2019.
- 1065 Hendrick, F., Müller, J.-F., Clémer, K., Wang, P., De Mazière, M., Fayt, C., Gielen, C., Hermans, C., Ma, J. Z., Pinardi, G., Stavrou, T., Vlemmix, T., and Van Roozendael, M.: Four years of ground-based MAX-DOAS observations of HONO and NO₂ in the Beijing area, *Atmos. Chem. Phys.*, 14, 765–781, <https://doi.org/10.5194/acp-14-765-2014>, 2014.
- Hönninger, G., von Friedeburg, C., and Platt, U.: Multi axis differential optical absorption spectroscopy (MAX-DOAS), *Atmos. Chem. Phys.*, 4, 231–254, doi:10.5194/acp-4-231-2004, 2004.
- 1070 Hooyberghs, J., Mensink, C., Dumont, G. and Fierens, F., 2006. Spatial interpolation of ambient ozone concentrations from sparse monitoring points in Belgium. *Journal of Environmental Monitoring*, 8(11), pp.1129-1135.
- Ialongo, I., Virta, H., Eskes, H., Hovila, J., and Douros, J.: Comparison of TROPOMI/Sentinel 5 Precursor NO₂ observations with ground-based measurements in Helsinki, *Atmos. Meas. Tech. Discuss.*, <https://doi.org/10.5194/amt-2019-329>, in review, 2019.
- 1075 Irie, H., Takashima, H., Kanaya, Y., Boersma, K. F., Gast, L., Wittrock, F., Brunner, D., Zhou, Y., and Van Roozendael, M.: Eight-component retrievals from ground-based MAXDOAS observations, *Atmos. Meas. Tech.*, 4, 1027–1044, <https://doi.org/10.5194/amt-4-1027-2011>, 2011.
- Irie, H., Boersma, K. F., Kanaya, Y., Takashima, H., Pan, X., and Wang, Z. F.: Quantitative bias estimates for tropospheric NO₂ columns retrieved from SCIAMACHY, OMI, and GOME-2 using a common standard for East Asia, *Atmos. Meas. Tech.*, 5, 2403–2411, <https://doi.org/10.5194/amt-5-2403-2012>, 2012.
- 1080 Janssen, S., Dumont, G., Fierens, F. and Mensink, C., 2008. Spatial interpolation of air pollution measurements using CORINE



- land cover data. *Atmospheric Environment*, 42(20), pp.4884-4903.
- 1085 Judd, L. M., Al-Saadi, J. A., Szykman, J. J., Valin, L. C., Janz, S. J., Kowalewski, M. G., Eskes, H. J., Veefkind, J. P., Cede, A., Mueller, M., Gebetsberger, M., Swap, R., Pierce, R. B., Nowlan, C. R., Abad, G. G., Nehrir, A., and Williams, D.: Evaluating Sentinel-5P TROPOMI tropospheric NO₂ column densities with airborne and Pandora spectrometers near New York City and Long Island Sound, *Atmos. Meas. Tech.*, 13, 6113–6140, <https://doi.org/10.5194/amt-13-6113-2020>, 2020.
- 1090 Khomenko, S., Cirach, M., Pereira-Barboza, E., Mueller, N., Barrera-Gómez, J., Rojas-Rueda, D., de Hoogh, K., Hoek, G. and Nieuwenhuijsen, M., 2021. Premature mortality due to air pollution in European cities: a health impact assessment. *The Lancet Planetary Health*, 5(3), pp.e121-e134.
- Klimont, Z., Kupiainen, K., Heyes, C., Purohit, P., Cofala, J., Rafaj, P., Borcken-Kleefeld, J., and Schöpp, W.: Global anthropogenic emissions of particulate matter including black carbon, *Atmos. Chem. Phys.*, 17, 8681–8723, <https://doi.org/10.5194/acp-17-8681-2017>, 2017.
- 1095 Kreher, K., Van Roozendaal, M., Hendrick, F., Apituley, A., Dimitropoulou, E., Frieß, U., Richter, A., Wagner, T., Abuhassan, N., Ang, L., Anguas, M., Bais, A., Benavent, N., Bösch, T., Bogner, K., Borovski, A., Bruchkouski, I., Cede, A., Chan, K. L., Donner, S., Drosoglou, T., Fayt, C., Finkenzeller, H., Garcia-Nieto, D., Gielen, C., Gómez-Martín, L., Hao, N., Herman, J. R., Hermans, C., Hoque, S., Irie, H., Jin, J., Johnston, P., Khayyam Butt, J., Khokhar, F., Koenig, T. K., Kuhn, J., Kumar, V., Lampel, J., Liu, C., Ma, J., Merlaud, A., Mishra, A. K., Müller, M., Navarro-Comas, M., Ostendorf, M., Pazmino, A., Peters, E., Pinardi, G., Pinharanda, M., Piter, A., Platt, U., Postlyakov, O., Prados-Roman, C., 1100 Puentedura, O., Querel, R., Saiz-Lopez, A., Schönhardt, A., Schreier, S. F., Seyler, A., Sinha, V., Spinei, E., Strong, K., Tack, F., Tian, X., Tiefengraber, M., Tirpitz, J.-L., van Gent, J., Volkamer, R., Vrekoussis, M., Wang, S., Wang, Z., Wenig, M., Wittrock, F., Xie, P. H., Xu, J., Yela, M., Zhang, C., and Zhao, X.: Intercomparison of NO₂, O₄, O₃ and HCHO slant column measurements by MAX-DOAS and zenith-sky UV-Visible spectrometers during the CINDI-2 campaign, *Atmos. Meas. Tech. Discuss.*, <https://doi.org/10.5194/amt-2019-157>, in review, 2019.
- 1105 Kurucz, R.L., Furenlid, I., Brault, J., and Testerman, L.: Solar flux atlas from 296 to 1300 nm, National Solar Observatory, Sunspot, New Mexico, U.S.A., 1984.
- Meller, R. and Moortgat, G. K.: Temperature dependence of the absorption cross sections of formaldehyde between 223 and 323K in the wavelength range 225–375nm, *J. Geophys. Res.*, 105, 7089–7101, 2000.
- Merlaud, A.: Development and use of compact instruments for tropospheric investigations based on optical spectroscopy from mobile platforms, Presses Universitaires de Louvain, 2013.
- 1110 Pinardi, G., Hendrick, F., Clémer, K., Lambert, J. C., Bai, J., and Van Roozendaal, M.: On the use of the MAX-DOAS technique for the validation of tropospheric NO₂ column measurements from satellite, *Proc. Eumetsat Conf.*, ISBN 978-92-9110-082-8, 2008.
- 1115 Puķīte, J., Kühl, S., Deutschmann, T., Platt, U., and Wagner, T.: Extending differential optical absorption spectroscopy for limb measurements in the UV, *Atmos. Meas. Tech.*, 3, 631–653, <https://doi.org/10.5194/amt-3-631-2010>, 2010.



- Quaas, Johannes, Olivier Boucher, Nicolas Bellouin, and Stefan Kinne. "Satellite-based estimate of the direct and indirect aerosol climate forcing." *Journal of Geophysical Research: Atmospheres* 113, no. D5 (2008).
- Rodgers, C. D.: Inverse Methods for Atmospheric Sounding, Theory and Practice, World Scientific Publishing, Singapore – New Jersey – London – Hong Kong, 2000.
- 1120 Rothman, L.S., Gordon, I.E., Babikov, Y., Barbe, A., Benner, D.C., Bernath, P.F., Birk, M., Bizzocchi, L., Boudon, V., Brown, L.R. and Campargue, A., 2013. The HITRAN2012 molecular spectroscopic database. *Journal of Quantitative Spectroscopy and Radiative Transfer*, 130, pp.4-50. Seinfeld, J. H. and Pandis, S. N.: Atmospheric Chemistry and Physics: From Air Pollution to Climate Change, John Wiley & Sons, Inc., 1998.
- Schreier, S. F., Bösch, T., Richter, A., Lange, K., Revesz, M., Weihs, P., Vrekoussis, M., and Lotteraner, C.: Evaluation of UV-visible MAX-DOAS aerosol profiling products by comparison with ceilometer, sun photometer, and in situ observations in Vienna, Austria, *Atmos. Meas. Tech.*, 14, 5299–5318, <https://doi.org/10.5194/amt-14-5299-2021>, 2021.
- 1125 Serdyuchenko, A., Gorshelev, V., Weber, M., Chehade, W., and Burrows, J. P.: High spectral resolution ozone absorption crosssections – Part 2: Temperature dependence, *Atmos. Meas. Tech.*, 7, 625–636, [doi:10.5194/amt-7-625-2014](https://doi.org/10.5194/amt-7-625-2014), 2014.
- Sinreich, R., Volkamer, R., Filsinger, F., Frieß, U., Kern, C., Platt, U., Sebastián, O., and Wagner, T.: MAX-DOAS detection of glyoxal during ICARTT 2004, *Atmos. Chem. Phys.*, 7, 1293–1303, <https://doi.org/10.5194/acp-7-1293-2007>, 2007.
- 1130 Sinreich, R., Merten, A., Molina, L., and Volkamer, R.: Parameterizing radiative transfer to convert MAX-DOAS dSCDs into near-surface box-averaged mixing ratios, *Atmos. Meas. Tech.*, 6, 1521–1532, [doi:10.5194/amt-6-1521-2013](https://doi.org/10.5194/amt-6-1521-2013), 2013.
- Spurr, R. J.: VLIDORT: A linearized pseudo-spherical vector discrete ordinate radiative transfer code for forward model and retrieval studies in multilayer multiple scattering media, *J. Quant. Spectrosc. Ra.*, 102, 316–342, 2006.
- 1135 Tack, F., Merlaud, A., Iordache, M.-D., Danckaert, T., Yu, H., Fayt, C., Meuleman, K., Deutsch, F., Fierens, F., and Van Roozendael, M.: High-resolution mapping of the NO₂ spatial distribution over Belgian urban areas based on airborne APEX remote sensing, *Atmos. Meas. Tech.*, 10, 1665–1688, <https://doi.org/10.5194/amt-10-1665-2017>, 2017.
- Tack, F., Merlaud, A., Meier, A. C., Vlemmix, T., Ruhtz, T., Iordache, M.-D., Ge, X., van der Wal, L., Schuettmeyer, D., Ardelean, M., Calcan, A., Constantin, D., Schönhardt, A., Meuleman, K., Richter, A., and Van Roozendael, M.: Intercomparison of four airborne imaging DOAS systems for tropospheric NO₂ mapping – the AROMAPEX campaign, *Atmos. Meas. Tech.*, 12, 211–236, <https://doi.org/10.5194/amt-12-211-2019>, 2019.
- 1140 Tack, F., Merlaud, A., Iordache, M.-D., Pinardi, G., Dimitropoulou, E., Eskes, H., Bomans, B., Veeffkind, P., and Van Roozendael, M.: Assessment of the TROPOMI tropospheric NO₂ product based on airborne APEX observations, *Atmos. Meas. Tech.*, 14, 615–646, <https://doi.org/10.5194/amt-14-615-2021>, 2021.
- 1145 Thalman, R. and Volkamer, R.: Temperature dependent absorption cross-sections of O₂-O₂ collision pairs between 340 and 630nm and at atmospherically relevant pressure, *Phys. Chem. Chem. Phys.*, 15, 15371–15381, [doi:10.1039/C3CP50968K](https://doi.org/10.1039/C3CP50968K), 2013.
- Tirpitz, J.-L., Frieß, U., Hendrick, F., Alberti, C., Allaart, M., Apituley, A., Bais, A., Beirle, S., Berkhout, S., Bognar, K., Bösch, T., Bruchkouski, I., Cede, A., Chan, K. L., den Hoed, M., Donner, S., Drosoglou, T., Fayt, C., Friedrich, M. M.,



- 1150 Frumau, A., Gast, L., Gielen, C., Gomez-Martín, L., Hao, N., Hensen, A., Henzing, B., Hermans, C., Jin, J., Kreher, K.,
Kuhn, J., Lampel, J., Li, A., Liu, C., Liu, H., Ma, J., Merlaud, A., Peters, E., Pinardi, G., Piters, A., Platt, U., Puentedura,
O., Richter, A., Schmitt, S., Spinei, E., Stein Zweers, D., Strong, K., Swart, D., Tack, F., Tiefengraber, M., van der Hoff,
R., van Roozendaal, M., Vlemmix, T., Vonk, J., Wagner, T., Wang, Y., Wang, Z., Wenig, M., Wiegner, M., Wittrock,
F., Xie, P., Xing, C., Xu, J., Yela, M., Zhang, C., and Zhao, X.: Intercomparison of MAX-DOAS vertical profile retrieval
1155 algorithms: studies on field data from the CINDI-2 campaign, *Atmos. Meas. Tech.*, 14, 1–35,
<https://doi.org/10.5194/amt-14-1-2021>, 2021.
- van Geffen, J. H. G., Eskes, H. J., Boersma, K. F., Maasackers, J. D., and Veeffkind, J.P.: TROPOMI ATBD of the total and
tropospheric NO₂ data products, KNMI, 2019.
- van Geffen, J. H. G., Eskes, H. J., Boersma, K. F., and Veeffkind, J.P.: TROPOMI ATBD of the total and tropospheric NO₂
1160 data products, Tech. Rep. S5P-KNMI-L2-0005-RP, Koninklijk Nederlands Meteorologisch Instituut (KNMI), <https://sentinels.copernicus.eu/documents/247904/2476257/Sentinel-5P-TROPOMI-ATBD-NO2-data-products>, CI-7430-
ATBD, issue 2.2.0, 16 June 2021.
- Van Geffer, J. H. G., Eskes, H. J., Compernelle, S., Pinardi, G., Verhoelst, T., Lambert, J.-C., Sneep, M., ter Linden, M.,
Ludewig, A., Boersma, K. F., and Veeffkind, J.P.: S5P/TROPOMI NO₂ retrieval: impact of version v2.2 improvements
1165 and preliminary comparisons with OMI and ground-based data, in preparation.
- Vandaele, A., Hermans, C., Simon, P., Carleer, M., Colin, R., Fally, S., Mérienne, M., Jenouvrier, A., and Coquart, B.:
Measurements of the NO₂ absorption cross-section from 42000cm⁻¹ to 10000cm⁻¹ (238–1000nm) at 220K and 294K,
J. Quant. Spectrosc. Ra., 59, 171–184, 1998.
- Veeffkind, J. P., Boersma, K. F., Wang, J., Kurosu, T. P., Krotkov, N., Chance, K., and Levelt, P. F.: Global satellite analysis
1170 of the relation between aerosols and short-lived trace gases, *Atmos. Chem. Phys.*, 11, 1255–1267, doi:10.5194/acp-11-
1255-2011, 2011.
- Verhoelst, T., Compernelle, S., Pinardi, G., Lambert, J.-C., Eskes, H. J., Eichmann, K.-U., Fjæraa, A. M., Granville, J.,
Niemeijer, S., Cede, A., Tiefengraber, M., Hendrick, F., Pazmiño, A., Bais, A., Bazureau, A., Boersma, K. F., Bogner,
K., Dehn, A., Donner, S., Elokhov, A., Gebetsberger, M., Goutail, F., Grutter de la Mora, M., Gruzdev, A., Gratsea, M.,
1175 Hansen, G. H., Irie, H., Jepsen, N., Kanaya, Y., Karagkiozidis, D., Kivi, R., Kreher, K., Levelt, P. F., Liu, C., Müller,
M., Navarro Comas, M., Piters, A. J. M., Pommereau, J.-P., Portafaix, T., Prados-Roman, C., Puentedura, O., Querel,
R., Remmers, J., Richter, A., Rimmer, J., Rivera Cárdenas, C., Saavedra de Miguel, L., Sinyakov, V. P., Stremme, W.,
Strong, K., Van Roozendaal, M., Veeffkind, J. P., Wagner, T., Wittrock, F., Yela González, M., and Zehner, C.: Ground-
based validation of the Copernicus Sentinel-5P TROPOMI NO₂ measurements with the NDACC ZSL-DOAS, MAX-
1180 DOAS and Pandonia global networks, *Atmos. Meas. Tech.*, 14, 481–510, <https://doi.org/10.5194/amt-14-481-2021>,
2021.
- Vigouroux, C., Hendrick, F., Stavrou, T., Dils, B., De Smedt, I., Hermans, C., Merlaud, A., Scolas, F., Senten, C.,
Vanhaelewyn, G., Fally, S., Carleer, M., Metzger, J.-M., Müller, J.-F., Van Roozendaal, M., and De Mazière, M.:



- 1185 Ground-based FTIR and MAX-DOAS observations of formaldehyde at Réunion Island and comparisons with satellite
and model data, *Atmos. Chem. Phys.*, 9, 9523–9544, <https://doi.org/10.5194/acp-9-9523-2009>, 2009.
- Wagner, T., Deutschmann, T., and Platt, U.: Determination of aerosol properties from MAX-DOAS observations of the Ring
effect, *Atmos. Meas. Tech.*, 2, 495–512, <https://doi.org/10.5194/amt-2-495-2009>, 2009.
- Wagner, T., Beirle, S., Brauers, T., Deutschmann, T., Frieß, U., Hak, C., Halla, J. D., Heue, K. P., Junkermann, W., Li, X.,
Platt, U., and Pundt-Gruber, I.: Inversion of tropospheric profiles of aerosol extinction and HCHO and NO₂ mixing
1190 ratios from MAX-DOAS observations in Milano during the summer of 2003 and comparison with independent data sets,
Atmos. Meas. Tech., 4, 2685–2715, <https://doi.org/10.5194/amt-4-2685-2011>, 2011.
- Wagner, T., Beirle, S., Benavent, N., Bösch, T., Chan, K. L., Donner, S., Dörner, S., Fayt, C., Frieß, U., García-Nieto, D.,
Gielen, C., González-Bartolome, D., Gomez, L., Hendrick, F., Henzing, B., Jin, J. L., Lampel, J., Ma, J., Mies, K.,
Navarro, M., Peters, E., Pinardi, G., Puentedura, O., Puķite, J., Remmers, J., Richter, A., Saiz-Lopez, A., Shaiganfar, R.,
1195 Sihler, H., Van Roozendael, M., Wang, Y., and Yela, M.: Is a scaling factor required to obtain closure between measured
and modelled atmospheric O₄ absorptions? An assessment of uncertainties of measurements and radiative transfer
simulations for 2 selected days during the MAD-CAT campaign, *Atmos. Meas. Tech.*, 12, 2745–2817,
<https://doi.org/10.5194/amt-12-2745-2019>, 2019.
- Wang, Y., Li, A., Xie, P. H., Wagner, T., Chen, H., Liu, W. Q., and Liu, J. G.: A rapid method to derive horizontal distributions
1200 of trace gases and aerosols near the surface using multi-axis differential optical absorption spectroscopy, *Atmos. Meas.*
Tech., 7, 1663–1680, <https://doi.org/10.5194/amt-7-1663-2014>, 2014.
- Wang, Y., Pukite, J., Wagner, T., Donner, S., Beirle, S., Hilboll, A., Vrekoussis, M., Richter, A., Apituley, A., Pipers, A.,
Allaart, M., Eskes, H., Frumau, A., Roozendael, M. V., Lampel, J., Platt, U., Schmitt, S., Swart, D., and Vonk, J.: Vertical
Profiles of Tropospheric Ozone From MAX-DOAS Measurements During the CINDI-2 Campaign: Part 1 –
1205 Development of a New Retrieval Algorithm, *J. Geophys. Res.-Atmos.*, 123, 10637–10670,
<https://doi.org/10.1029/2018JD028647>, 2018.
- Williams, J.E., Boersma, K.F., LeSager, P., and Verstraeten, W.W.: The high-resolution version of TM5-MP for optimized
satellite retrievals: description and validation, *Geosci. Model Dev.*, 10, 721–750, [https://doi.org/10.5194/gmd-10-721-](https://doi.org/10.5194/gmd-10-721-2017)
2017, 2017.
- 1210 Wittrock, F., Oetjen, H., Richter, A., Fietkau, S., Medeke, T., Rozanov, A., and Burrows, J. P.: MAX-DOAS measurements
of atmospheric trace gases in Ny-Ålesund - Radiative transfer studies and their application, *Atmos. Chem. Phys.*, 4, 955–
966, <https://doi.org/10.5194/acp-4-955-2004>, 2004.

1215